The effects of 17α-estradiol treatment on endocrine system revealed by single-nucleus transcriptomic sequencing of hypothalamus

Lei Li[#,*1], Guanghao Wu[#2], Xiaolei Xu[3], Junling Yang[4], Lirong Yi[5], Ziqing Yang[6], Zheng Mo[3], Li Xing[3], Ying Shan[*1], Zhuo Yu[*3], Yinchuan Li[*5]

[1]Department of Obstetrics and Gynecology, National Clinical Research Center for Obstetric & Gynecologic Diseases, Peking Union Medical College Hospital, Chinese Academy of Medical Sciences and Peking Union Medical College, 100730 Beijing, China.

[2]School of Medical Technology，Beijing Institute of Technology, 100081, Beijing, China.

[3]Department of Medical Oncology，Beijing Tsinghua Changgung Hospital, School of Clinical Medicine, Tsinghua University, 102218, Beijing, China.

[4]Department of Cancer Biology and Pharmacology, University of Illinois College of Medicine, Peoria, Illinois, United states of America.

[5]Institute of Reproductive Medicine, Medical School of Nantong University, Nantong, Jiangsu 226001, China.

[6]School of Basic Medical Sciences, Shandong University, Jinan, Shandong 250012, China.

# These authors contributed equally: Lei Li, Guanghao Wu

* Corresponding author. Email: shypumch@163.com; lilei64@pumch.cn; yza02214@btch.edu.cn; 18622397604@163.com

Abstract

In this study, we investigated the role of 17α-estradiol in lifespan extension and its potential side effects from long-term administration. Pooled hypothalami from aged male Norway brown rats treated with 17α-estradiol (O.T), aged male controls (O), and young male controls (Y) were subjected to single-nucleus transcriptomic sequencing (snRNA-seq). To evaluate the effects of 17α-estradiol on aging neurons, supervised clustering of neurons based on neuropeptides and their receptors were used to evaluate the responses of each neuron subtype during aging and after 17α-estradiol treatment. The elevated cellular metabolism, stress and decreased expression levels of pathways involved in synapse formation in neurons initiated by aging were significantly

attenuated by 17α-estradiol. Assessment of changes in neuron populations showed that neurons related to food intake, reproduction, blood pressure, stress response, and electrolyte balance were sensitive to 17α-estradiol treatment. 17α-estradiol treatment not only increased serum Oxytocin (Oxt), but also heightened the activity of hypothalamic-pituitary-gonadal (HPG) axis, as evidenced by significantly elevated levels of plasma Gnrh, total testosterone, and decreased estradiol. Elevated Gnrh1 was confirmed to be one of the causal effects mediating the role of 17α-estradiol in energy homeostasis, neural synapse, and stress response. Notably, *Crh* neurons exhibited prominent stressed phenotype among all the checked neuron subtypes in O.T, which may indicate a potential side effect of 17α-estradiol treatment. Therefore, the HPG axis and energy metabolism may be key targets of 17α-estradiol in male hypothalamus. Additionally, supervised clustering of neurons was shown to be a useful method for assessing treatment responses among different neuron subtypes in the hypothalamus.

Key words snRNA-seq, hypothalamus, 17α-estradiol, aging, Crh, Oxt, Gnrh

Background

The hypothalamus serves as the central hub for controlling energy homeostasis, stress response, temperature, learning, feeding, sleep, social behavior, sexual behavior, hormone secretion, reproduction, osmoregulation, blood pressure, visceral activities, emotion, and circadian rhythms [1]. The hypothalamic energy-sensing system, particularly the circuits that regulate food intake, plays a crucial role in life span extension [2]. Elevated metabolic activity in the aged hypothalamus has been reported in aged hypothalamus, including increased mTor signaling [3, 4]. Additionally, decreases in gonadotropin-releasing hormone (GnRH), Ghrh, Trh, monoamine neurotransmitters, and blood supply are hallmarks of aging hypothalamus [5].

Previous studies have demonstrated that 17α-estradiol extends the lifespan of male mice and has beneficial effects on metabolism and inflammation, similar to those of rapamycin and acarbose [6-8]. Recent study indicated that 17α-estradiol also extends the lifespan of male rats [9].Further investigations revealed certain unique features of 17α-estradiol in life extension distinct to rapamycin and acarbose [10, 11]. Moreover, it has been shown that 17α-estradiol targets hypothalamic *POMC* neurons to reduce metabolism by decreasing feeding behavior through anorexigenic pathways [12]. Interestingly, the lifespan extension effect has only been observed in

male animals [13]. The safety of 17α-estradiol is key for translation into clinical treatment, and the potential side effects on reproduction and feminization by 17α-estradiol treatment must be considered. However, contradictory results have been reported regarding its side effects on reproduction and feminization [6, 14, 15]. Therefore, further investigation and verification are needed to understand the underlying mechanisms of lifespan extension and the safety of 17α-estradiol.

In this report, we utilized single-nucleus transcriptomic sequencing and performed supervised clustering of neurons based on neuropeptides, hormones, and their receptors. Supervised clustering offers better resolution in cell cluster screening compared to traditional unsupervised clustering. We assessed the effects of 17α-estradiol on metabolism, stress responses, ferroptosis, senescence, inflammation, and pathways involved in synaptic activity in each neuron subtype, ranking the most sensitive neurons. The effects of 17α-estradiol on reversing aging-related cellular processes were evaluated by two opposing regulatory networks involved in hypermetabolism, stress, inflammation, and synaptic activity. Several key endocrine factors from serum were examined, and the potential side effects of 17α-estradiol on specific neurons were also evaluated.

Materials and methods

Animals, treatment and tissues

Twelve Norway brown male rats (12 months old) were acquired from Charles River, including 8 12-months old and 4 1-month old (Beijing). Aged rats were randomly allocated into control and 17α-estradiol-treated groups. Four Aged rats treated with 17α-estradiol (Catalog #: E834897, Macklin Biochemical, Shanghai, China) were fed freely with regular diet mixed with 17α-estradiol at a dose of 14.4 mg/kg (14.4 ppm), starting at 24 months of age for 6 months according to prior reports [16, 17]. The young rats were fed a regular diet without 17α-estradiol continuously for 3 months until 4 months old. All rats had ad libitum access to food and water throughout the experiments. The rats were then euthanized via CO_2, hypothalami, testes and blood serum were collected for subsequent experimental procedures. All blood samples were collected at 9:00-9:30 a.m to minimize hormone fluctuation between animals. All animal procedures were reviewed and approved by the Institutional Animal Care and Use Committee at Nantong University.

Enzyme immunoassays

Enzyme immunoassays kits for rat Oxt (Catalog #: EIAR-OXT), Corticotropin Releasing Factor (Catalog #: EIAR-CRF), and gonadoliberin-1 (Catalog #: EIAR-GNRH) were obtained from Raybiotech (GA, USA). Enzyme immunoassay kits for rat serum total testosterone (Catalog #: ml002868), estradiol (Catalog #: ml002891), aldosterone (Catalog #: ml002876), and cortisol (Catalog #: ml002874) were obtained from Enzyme-linked Biotechnology (Shanghai, China). Sera from 3 animals per group were used and each was diluted 10 or 20 times for immunoassays.

Seminiferous tubule inflammation test

8 testes were obtained from each sample group and then subjected to fixation in 4% formalin for at least 1 week. Formalin-fixed paraffin-embedded mouse testis sections of 5 μm thickness were used for HE Staining. At least 30 seminiferous tubules in each slide were examined for inflammation test. Testis with at least 1 inflammatory seminiferous tubule was set as 1, and normal testis was set as 0 for inflammation index calculation.

snRNA-seq data processing, batch effect correction, and cell subset annotation

Intact hypothalami were cryopreserved in liquid nitrogen from sacrificed rats. Two (O) or three (Y and O.T) hypothalami were pooled within each group and homogenized in 500 μL ice-cold homogenization buffer (0.25 M sucrose, 5 mM $CaCl_2$, 3 mM $MgAc_2$, 10 mM Tris-HCl [pH 8.0], 1 mM DTT, 0.1 mM EDTA, 1× protease inhibitor, and 1 U/μL RiboLock RNase inhibitor) with Dounce homogenizer. Then, the homogenizer was washed with 700 μL ice-cold nuclei washing buffer (0.04% bovine serum albumin, 0.2 U/μL RiboLock RNase Inhibitor, 500 mM mannitol, 0.1 mM phenylmethanesulfonyl fluoride protease inhibitor in 1× phosphate buffer saline). Next, the homogenates were filtered through a 70-μm cell strainer to collect the nuclear fraction. The nuclear fraction was mixed with an equal volume of 50% iodixanol and added on top of a 30% and 33% iodixanol gradient. This solution was then centrifuged for 20 min at 10 000 ×g at 4 °C. After the myelin layer was removed from the top of the gradient, the nuclei were collected from the 30% and 33% iodixanol interface. The nuclei were resuspended in nuclear wash buffer and resuspension buffer and pelleted for 5 min at 500 ×g at 4 °C. The nuclei were filtered through a 40-μm cell strainer to remove cell debris and large clumps, and the nuclear concentration was manually assessed using trypan blue counterstaining and a hemocytometer. Finally, the nuclei were adjusted to 700–1200 nuclei/μL, and examined with a 10X Chromium platform.

Reverse transcription, cDNA amplification and library preparation were performed according to the protocol from 10X Genomics and Chromium Next GEM Single Cell 3′ Reagent Kits v3.1. Library sequencing was performed on the Illumina HiSeq™ 4000 by Gene Denovo Biotechnology Co., Ltd (Guangzhou, China).

10X Genomics Cell Ranger software (version 3.1.0) was used to convert raw BCL files to FASTQ files, and for alignment and counts quantification. Reads with low-quality barcodes and UMIs were filtered out and then mapped to the reference genome. Reads uniquely mapped to the transcriptome and intersecting an exon at least 50% were considered for UMI counting. Before quantification, the UMI sequences were corrected for sequencing errors, and valid barcodes were identified using the EmptyDrops method. The cell × gene matrices were produced via UMI counting and cell barcodes calling. Cells with an unusually high number of UMIs (≥8000) or mitochondrial gene percent (≥15%) were filtered out. Batch effect correction was performed by SCTransform function built in Seurat V4.4.0.

Pathways, gene signatures, TFs and TF cofactors, cell communication

Gene sets and pathways were derived from Hallmark gene sets of MSigDB collections, the KEGG pathway database, Reactome pathway database, and WikiPathways database, and some ontology terms derived from the Gene Ontology (GO) resource. Mitochondrial pathways were derived from MitoCarta3.0 [18]. Pathways, gene sets, and gene signatures were evaluated with the PercentageFeatureSet function built into R package Seurat. TFs and TF cofactors were obtained from AnimalTFDB 3.0 [19]. TFs and TF cofactors were further filtered with mean counts >0.1.

The ligand–receptor pairs were calculated via R package CommPath [20].

Correlation analysis and ROC analysis

Pearson correlation coefficient was calculated with the linkET package ($p < 0.05$). Fast Wilcoxon rank sum test and auROC analysis was performed with the wilcoxauc function in R package presto. The minimal cell number in either one of the comparing pairs should be no less than 15. Ranks of area under the curve (AUC) values were in descending order. A total of 431 pathways from Hallmark, KEGG and PID databases were used for correlation analysis with MitoCarta OXPHOS subunits in neurons and non-neural cells (**Figure 2—figure supplement 1**). A total of 97 pathways related to synapse activity were derived from GO, including GO cellular components, GO biological processes and GO molecular functions (**Table S1**).

The division of expression level-dependent clusters in each pathway and their gene signatures

The quarters of the mixed cell populations from O, O.T, and Y hypothalamic neurons were equally divided using the R function fivenum from the R package stats, based on pathway expression levels. Thus, the total number of neurons was evenly divided into four clusters (c1-c4) in terms of cell number. The cell proportions from O.T, O, and Y neurons in each cluster were weighted against the total number of neurons in the three groups. The unique markers of each cluster were calculated using the FindAllMarkers function from the Seurat package. The intersection of the unique markers from the six pathways was obtained for heatmap plotting. Nineteen genes that were highly expressed in c1 were identified as c1.up.signature via the PercentageFeatureSet function in the Seurat package. Twelve genes that were highly expressed in c4 were identified as c4.up.signature. There were no intersecting unique markers in clusters c2 and c3 among the six selected pathways.

TF and pathway activities

The TF resources were derived from CollecTRI, the pathway resource was from PROGENy, and the enrichment scores of TFs and pathways were performed with the Univariate Linear Model (ulm) method according to the pipeline in R package decoupleR [21].

Subtypes of neurons generated by supervised clustering

Vast majority of these subtypes were clustered by neuropeptides, hormones, and their receptors within all the neurons with the subset function from R package Seurat (the target gene expression level > 0). A total of 121 neuron subtypes were obtained, comprising 80 neuropeptide-secreting neurons and 41 neurons expressing a unique neuropeptide receptor or hormone receptor. Further groupings may exist within the identified neuron subtypes, and the category of excitatory or inhibitory neurons was not discriminated further. The cell proportion of each neuron subtype was weighted according to the total number of neurons in O.T, O, and Y samples. The mean values ± standard deviation of pathways and gene signatures were performed for each subtype. The top 10 and the bottom 10 items were calculated, and the top 10 subtypes ranked within each of 16 pathways or gene signatures were collected for word clouds annotation via R package wordcloud2.

Differential expression and pathway enrichment analysis

DEGs between groups were identified via FindMarkers (test.use = bimod, min.pct = 0.1, logfc.Threshold = 0.25, avg_diff > 0.1 or < −0.1). DEGs were then enriched in redundant GO terms via WebGestalt and filtered with false discovery rate < 0.05 [22].

Bidirectional Mendelian randomization (MR) study

The protein quantitative trait locus (pQTL) GWAS summary data of 204 human endocrine-related GWAS summary data with European ancestry were obtained from open-access MRC Integrative Epidemiology Unit (IEU) (**Table S4**) [23, 24]. Independent genome-wide significant SNPs for exposure OXT (id:prot-a-2159) or GNRH1 (id: prot-a-1233) were used as instrumental variables with genome-wide significance ($P < 1 \times 10^{-5}$), independence inheritance (r2 < 0.001) without linkage disequilibrium (LD) with each other for MR. For the reverse MR, independent genome-wide significant SNPs from 203 endocrine-related GWAS summary data ($P < 1 \times 10^{-5}$, r2 < 0.001) without LD with each other were obtained as exposures and human GWAS summary data of OXT (id:prot-a-2159) or GNRH1 (id:prot-a-1233) were used as outcomes. Weak instruments less than 10 were discarded via F-statistics.

MR and reverse MR analysis were conducted with method inverse-variance weighting (IVW), MR Egger, Weighted median, Simple mode, and Weighted mode. The screening criteria: all of the odds ratio (OR) values of the 5 methods should be simultaneously either >1 or <1 and the significant p value of IVW was <0.05. The heterogeneity via IVW method and the horizontal pleiotropy were also evaluated with R package TwoSampleMR [25].

Results

The overall changes in aged hypothalamus with or without long-term 17α-estradiol treatment via snRNA-seq profiling

To investigate the hypothalamus as a potential key target of 17α-estradiol's effects on life extension, we performed snRNA-seq on the entire hypothalamus of aged and 17α-estradiol-treated aged Norway brown rats, using the hypothalamus from young adult male rats as a control. We identified 10 major cell types based on specific cell markers of the hypothalamus (**Figure 1A-B**). Notably, the proportions of all non-neural cells changed in O versus Y (**Figure 1C**). For instance, Oligo, OPC, and Micro were found to be increased, while Astro, Tany, Fibro, PTC, and Endo were decreased in O compared to Y. The proportions of Oligo, OPC, and Micro were also increased in

17α-estradiol-treated aged group (O.T) compared to those in Y. Furthermore, Endo was increased in O.T compared to both Y and O. The proportions of Astro, Tany, Epen, and PTC decreased more in O.T than those in O when compared to Y. These results indicated that 17α-estradiol treatment had extensive effects on the proportions of non-neural cells in hypothalamus.

Cell communication analysis revealed significant changes in the ligand-receptor pairs between neurons and other cell types, particularly in Endo, Fibro, Tany, and Astro (**Figure 1D**). Significant ligand–receptor interactions among neurons also changed in O.T and O groups, especially in O (**Figure 1E**). Notably, among the significant ligand–receptor pairs in neurons, *Bmp2–Acvr1/Acvr2a/Acvr2b/Bmpr*, *Gdf11–Acvr2a/Acvr2b*, *Inhba–Acvr1/Acvr2a/Acvr2b*, *Nrg1/Nrg2/Nrg4–Erbb4*, *Rspo1–Lgr5/Lrp6*, and *Rspo3–Lgr5* were exclusively and significantly increased in neurons of the O group compared to those in O.T and Y, suggesting enhanced TGF superfamily-mediated signaling activity and canonical Wnt signaling during aging. The significantly changed ligand–receptor pairs *Nlgn1–Nrxn1/Nrxn2*, *Nlgn2–Nrxn1/Nrxn2/Nrxn3*, *Nlgn3–Nrxn1/Nrxn2/Nrxn3*, *Nxph1–Nrxn1/Nrxn2/Nrxn3*, *Nxph3–Nrxn1/Nrxn2/Nrxn3*, *Pomc–Oprd1/Oprk1/Oprm1*, and *Vip–Adcyap1r1/Avpr1a/Vipr2* were exclusively increased in neurons of O.T compared to O and Y (**Figure 1E**). These ligand–receptor pairs were associated with synaptic activity, cellular adhesion, the opioid system, and vasodilation, indicating unique roles of 17α-estradiol in restoring certain physiological functions in the aging hypothalamus. The increased *Pomc* signal in O.T neurons aligns with previous reports suggesting that 17α-estradiol treatment decreases food uptake in mice, potentially correlated with *Pomc* neurons (**Figure 1E**) [12].

Gene set enrichment analysis (GSEA) based on DEGs also corroborated the expression profiles related to stress responses and synapse-associated cellular processes in neurons (**Figure 1F**). ROC analysis of significantly differently expressed pathways related to neural synapses, manually selected from Gene Ontology databases, indicated that most top-ranked pathways related to synapses, according to AUC values, were downregulated in aged neurons, while 17α-estradiol treatment reversed this trend (**Figure 1G, Table S1**).

Overall, these findings suggest that 17α-estradiol broadly reshapes cell populations, cellular communication, neuropeptide secretion, and synapse-related cellular processes in the aging hypothalamus, distinguishing it from both the young hypothalamus and the untreated aged

hypothalamus.

The two opposing signaling networks in regulating metabolism and synapse activity, which can be balanced effectively by 17α-estradiol

To monitor the metabolism and neural status affected by 17α-estradiol, we utilized the energy metabolism pathway MitoCarta OXPHOS subunits to calculate the positively or negatively correlated pathways in hypothalamic neurons (**Figure 2—figure supplement 1**). Our findings revealed that energy metabolism and synapse activity represent two opposing regulatory signaling networks in hypothalamic neurons, with 17α-estradiol strongly playing a significant role in balancing these networks (**Figure 2A**). At the core of these opposing signaling pathways are two categories of contrasting TFs (**Figure 2B**). For example, *Calr*, *Clu*, *Peg3*, *Prnp*, *Ndufa13*, *Actb*, *Ywhab*, *Nfe2l1*, *Mtdh*, *Npm1*, *Bex2*, *Aft4*, and *Maged1* were positively correlated with pathways involved in OXPHOS subunits, lysosome function, protein export, mTorc1 signaling, and the unfolded protein response (UPR) in O, O.T and Y neurons, while showing negative correlations with pathways related to ubiquitin-mediated proteolysis, endocytosis, tight junctions, focal adhesion, axon guidance, and MAPK signaling. Additionally, TFs *Myt1l*, *Ctnnd2*, *Tenm4*, *Camta1*, *Med12l*, *Rere*, *Csrnp3*, *Erbb4*, *Jazf1*, *Dscam*, *Klf12*, and *Kdm4c* exhibited opposite correlation patterns with these selected pathways in O, O.T and Y neurons. These TFs may take conserved roles in regulating the two opposing biological processes in hypothalamic neurons.

We then attempted to establish gene signatures to represent these two opposing signaling networks, thereby displaying the cell status of aging and evaluating the effects exerted by 17α-estradiol. To achieve this, we evenly divided the expression levels of each of the six selected pathways from the two opposing signaling networks into four quarters (c1-c4) among the mixed neurons from O, O.T, and Y, calculating the shared unique markers in each quarter (**Figure 2C, D**). From the distribution patterns, we observed that the proportion of neurons in O decreased from c1 to c4 in metabolic pathways (MitoCarta OXPHOS subunits and Hallmark mTorc1 signaling), while this trend was reversed in the opposing signaling pathways (GOBP synapse organization and KEGG MAPK signaling pathway) (**Figure 2C**). In contrast, in Y, this trend was opposite, suggesting the expression levels from the 4 quarters (c1-c4) of the two opposing signaling networks can be used to monitor aging status. Treatment with 17α-estradiol alleviated this trend or even reversed it in O.

We then screened the shared unique markers of each quarter from the six selected pathways in an attempt to establish the gene signatures representing the two opposing signaling networks. Unique markers in c1 (19 genes, c1.up.signature) and c4 (12 genes, c4.up.signature) were identified; however, c2 and c3 lacked unique markers shared by the 6 pathways (**Figure 2D**). Consequently, the 19 genes in c1.up.signature displayed an inversed correlation pattern with the 12 genes in c4.up.signature, indicating the two opposing gene signatures are capable of reflecting the two opposing signaling networks in hypothalamic neurons (**Figure 2E**). Conversely, the balance of the two opposing signaling networks affected by 17α-estradiol in non-neural cell types was less pronounced than in neurons, showing variable effects on non-neural cells (**Figure 2—figure supplement 2**). GOBP pathway enrichment analysis revealed that Micro exhibited lower levels of synapse-related cellular processes in O.T compared to O, which was distinct from the observations in neurons (**Figure 2—figure supplement 3**). Therefore, in this report, we primarily focused on hypothalamic neurons and their responses to aging and 17α-estradiol.

Supervised clustering revealed distinct responses of different subtypes of hypothalamic neurons to aging and 17α-estradiol

The hypothalamus contains numerous neuron subtypes that release various neuropeptides and hormones to regulate fundamental body functions. To differentiate the changes occurring during aging and the effect of 17α-estradiol on each neuron subtype, we performed supervised clustering based on neuropeptides, hormones, or their receptors (**Figure 3A**). Most of the top 10 neuron subtypes involved in UPR, ferroptosis, mTorc1 signaling, insulin signaling pathway, immune response pathways, OXPHOS subunits, and senescence signature during aging were attenuated by 17α-estradiol treatment (**Figure 3B, Figure 3—figure supplement 1**). For example, Serpine1-secreting neurons exhibited very high expression levels of UPR, ferroptosis signature, mTorc1 signaling, Tnfα signaling via NF-kB, and OXPHOS subunits during aging, all of which were attenuated by 17α-estradiol.

To further identify the most sensitive neurons in response to aging and 17α-estradiol, we calculated the frequency of each neuron subtype by combining the top 10 neurons across each of the 16 pathways and gene signatures (**Figure 3C, Table S2**). Serpine1-secreting neurons were exclusively enriched in aged hypothalamus, suggesting they are effective targets of 17α-estradiol.

Additionally, *Mlnr*, *Nmb*, *Pomc*, *Ednra*, *Serpine3*, *Gast*, and *Pcsk6* neurons were all affected by 17α-estradiol (**Figure 3D**). *Galp*, *Glp1r*, *Serping1*, *Sstr2*, *Sstr3*, and *Vip* neurons were enriched in O, O.T and Y hypothalamus, indicating a lack of effect of 17α-estradiol on these neuron types. The unique neurons in O.T (*Crh*, *Serpinb9*, *Cckbr*, *Pth2r*, *Kiss1*, *Prpr*, *Hcrtr1*, *Npb*, *Nppa*, *Nxph3*, and *Npff*) may be a consequence of compensatory effects from 17α-estradiol treatment.

We then evaluated the most and least sensitive neurons to aging by ranking the neuron subtypes according to the levels of c1.up.signature and c4.up.signature (**Figure 3E**). *Serpine1*, *Galp*, *Calca* neurons were among the most affected subtypes in the aged hypothalamus, consistent with the combined ranks of several pathways (**Figure 3—figure supplement 1**). *Npr3*, *Crh*, *Ar*, *Esr1*, and *Esr2* neurons were among the least affected subtypes in the aged hypothalamus (**Figure 3E**). In O.T, neuron subtypes ranked by c1.up.signature and c4.up.signature indicated that *Gast*, *Npb*, *Nppa*, and *Crh* were affected most by 17α-estradiol treatment (**Figure 3F**). Neurons *Oxtr*, *Glp1r*, *Gnrh1*, and *Crh* also showed the lowest levels of c4.up.signature, indicative of an aging phenotype. Meanwhile, neurons *Glp2r*, *Ar* and *Esr1* ranked among the top neurons based on c4.up.signature, suggesting higher expression levels of synapse-related processes and relatively less stress status in these types of neurons in O.T.

These results indicate that supervised clustering of each neuron subtype of neurons facilitated the visualization of the different responses from distinct subtypes of neurons in response to aging and medical treatments. Furthermore, it strongly suggests that *Crh*, *Oxtr*, *Glp1r*, *Gnrh1*, *Glp2r*, *Ar*, and *Esr1* neuron subtypes are particularly sensitive to long-term 17α-estradiol treatment, which is associated with appetite regulation, glucose metabolism, stress response, and, as expected, sex hormone secretion and signaling.

The potential side effects on hypothalamic–pituitary–adrenal (HPA) axis by long-term 17α-estradiol treatment in the males

To further investigate the potential side effects or compensatory effects of 17α-estradiol treatment, we performed stricter screening by intersecting the top 10 ranks in the UPR, OXPHOS subunits, and ferroptosis signature (**Figure 4A**). *Crh* and *Nppa* were the only two intersected neuron subtypes identified through this strict screening. The treatment with 17α-estradiol elevated several key metabolic pathways in *Crh* neurons compared to those in Y and O (**Figure 4B**). Additionally,

17α-estradiol treatment increased the c1-up-signature while simultaneously reducing many pathways associated with synapse activity and the c4-up-signature in *Crh* neurons of O.T, indicating a potent stressed phenotype in *Crh* neuron. In contrast, in *Nppa* and *Nppc* neurons, the decreased c1-up-signature in O.T implied a lesser extent of stressed phenotype in these neurons compared to *Crh* neurons. The aberrant changes in *Crh* neurons were also evidenced by the increased number of DEGs related to mitochondria-expressed genes in O.T, along with a reduced number of DEGs in the adherens junction pathway (**Figure 4C**). The status of Crh neurons in O.T may be associated with elevated TF activities of *Esr2*, *Usf2*, *Hdac5*, *Creb3l1*, *Tfam*, *Preb*, *Pou3f2*, and *Hoxb5* (**Figure 4D**).

Notably, the HPA axis was altered by 17α-estradiol treatment, as evidenced by the elevated cortisol levels in O.T compared to O ($p = 0.078$) (**Figure 4E**). The correlation between elevated cortisol production and the heightened stress in *Crh* neurons by 17α-estradiol treatment needs further investigation. Additionally, as a crucial component of the renin-angiotensin-aldosterone system, the significantly increased serum aldosterone in O.T and its potential role in sodium reabsorption and cardiovascular health also warrant more detailed investigation (**Figure 4E**).

In summary, 17α-estradiol treatment altered the activity of HPA axis in male BN rats and introduced increased potential side effects in *Crh* neurons.

17α-estradiol increased Oxt neuron proportion and secretion and its possible role in mediating the effect of 17α-estradiol on endocrine system

Aging and 17α-estradiol treatment also altered the proportions of various neuron subtypes among O, O.T, and Y (**Figure 5A, B, Table S3**). The proportions of *Grp*, *Pmch*, *Npb*, *Serpinb9*, *Sstr2*, *Agrp*, *Sstr3*, *Mlnr*, and *Hcrt* neurons ranked in the top 10 in O, while *Oxt*, *Vip*, *Avp*, *Calca*, *Glp2r*, *Tacr1*, *Trh*, *Serping1*, *Npff*, and *Npy1r* were in the top 10 in O.T. *Galp*, *Calcrl*, *Ednra*, *Oxt*, *Serpinh1*, *Pomc*, *Cck*, *Crh*, *Tacr1*, and *Kiss1* neurons were among the bottom 10 in O, whereas *Oxtr*, *Galp*, *Agrp*, *Serpinb9*, *Npvf*, *Serpinh1*, *Ednrb*, *Agt*, *Gipr*, and *Pomc* neurons ranked among the bottom 10 in O.T. *Agrp*, *Pomc*, *Oxt*, *Oxtr*, *Gipr*, and *Glp2r* neurons are well-known for their roles in regulating food intake and energy homeostasis. *Agrp* neurons are activated by hunger, while *Pomc* neurons are activated by satiety in the ARC of the hypothalamus. 17α-estradiol treatment effectively elevated the expression levels of the c4.up.signature and synapse-associated

processes in neuron subtypes *Agrp*, *Pomc*, *Oxt* and *Glp2r* in O.T compared to O. This may mitigate the adverse effects of reduced cell populations in Pomc and *Agrp* neurons in aging hypothalamus (**Figure 5C**). This finding indicates a potential role of 17α-estradiol in appetite control, as previously reported [12]. Additionally, 17α-estradiol treatment resulted in elevated proportions of *Vip*, *Avp*, *Npff*, *Calca*, and *Tacr1* neurons, which ranked in the top 10, while the proportions of Agt neurons decreased. These are all associated with blood pressure regulation (**Figure 5—figure supplement 1**). Notably, the proportions of *Oxt* and *Glp2r* neurons, both of which have anorexigenic effects [26, 27], increased in O.T. In addition to the increased number of *Oxt*-positive neurons, the expression level of *Oxt* also rose in O.T. The elevated expression of synapse-related pathways was supported by the increased DEGs in the enriched synaptic membrane pathway in *Oxt* neurons (**Figure 5D**).

More importantly, the serum level of Oxt was significantly elevated in O.T compared to O (p=0.04), although it remained lower than that in Y (**Figure 5E**). Notably, the top TF activities in O.T and O differed markedly from those in Y (**Figure 5F**). The elevated levels of *Hopx* and *Xbp1* may be associated with the response to 17α-estradiol treatment.

Due to the intricate regulatory networks among various endocrine factors, elucidating the causal effect of Oxt on other endocrine factors is quite complex using traditional methods. MR analysis, employing variant SNPs as genetic tools, is advantageous for such task. We performed a bidirectional MR analysis of the GWAS summary data of human plasma OXT and 203 endocrine-related and hypothalamus-related factors, most of which are protein quantitative trait loci (pQTL) data from the IEU (**Table S4**). As an exposure, OXT revealed a significant causal effect on POMC/beta-endorphin (id:prot-a-2327, id:prot-a-2325), glucagon (id:prot-a-1181), GNRH1/Progonadoliberin-1 (id:prot-a-1233), and total testosterone levels (id:ebi−a−GCST90012112, id:ieu−b−4864) (**Figure 5G**). NPW and CBLN1 were found to be negatively associated with OXT, but the significance of these associations was not found in the reverse MR analysis (**Figure 5—figure supplement 2A, B**).

In contrast, we could not identify significant associations between OXT and estradiol levels (id:ebi-a-GCST90012105, id:ebi-a-GCST90020092, id:ebi-a-GCST90020091, id:ieu-b-4872, id:ieu-b-4873, id:ukb-e-30800_AFR, id:ukb-e-30800_CSA). Interestingly, QRFP, IGF1, AGRP, TAC4, GRP, CLU, BNF, PCSK7, PACAP, ANP, TAC3, CRH, INSL6, and PRL displayed

significant associations with OXT in both MR and reverse MR analysis, indicative of their complex causal effects (**Figure 5—figure supplement 2A, B**).

The results suggest that elevated Oxt levels induced by 17α-estradiol may have positive associations with endocrine factors governing feeding behavior, glucose metabolism, male reproduction, and sex hormones. Therefore, OXT may serve as a potential mediator of 17α-estradiol.

17α-estradiol activated HPG axis and the elevated Gnrh also took important roles in mediating the effect of 17α-estradiol on other endocrine factors

Since Gnrh and sex hormone expressing neuron subtypes were sensitive to 17α-estradiol treatment (**Figure 3F, Figure 3—figure supplement 1**), we examined their expression profiles alongside representative pathways of two opposing signaling networks related to metabolism and synapses, including c1-up-signature and c4-up-signature (**Figure 6A**). However, neither the c1-up-signature nor the c4-up-signature was up-regulated in *Gnrh1* neuron in the O.T, similar to the observations in *Esr2* neuron. Only in *Esr1* neuron was the c1-up-signature found to be up-regulated. Meanwhile, both *Ar* and *Esr* neurons displayed high level of c4-up-signature, indicating a relatively healthy status. The data suggest that most of the 4 types of sex hormone-related neurons did not experience severe aging in O.T. However, based on these expression profiles, it's difficult to define the precise physiological status of these subtypes of neurons, particularly regarding neuroendocrine activities. Consequently, we performed enzyme immunoassays of hormones from the serum of O, O.T and Y. The treatment with 17α-estradiol significantly increased the plasma level of Gnrh compared to Y ($p = 0.0099$) and approached significance when compared to O ($p = 0.096$) (**Figure 6B**). More intriguingly, testosterone levels in serum were significantly increased in O.T compared to O ($p = 0.018$) and approached significance when compared to Y ($p = 0.052$). Additionally, the serum estradiol levels were significantly increased in O compared to Y ($p = 0.011$) and significantly decreased in O.T compared to O ($p = 0.019$), suggesting that 17α-estradiol treatment markedly altered the homeostasis of testosterone and estradiol.

Furthermore, most testes from 30-month-old male BN rats exhibited severe age-related inflammation and epithelial collapse of seminiferous tubules (**Figure 6C**). The testes without inflammation in O.T displayed normal morphology. 17α-estradiol treatment slightly decreased the

testis inflammation in O.T compared to that in O (p = 0.15), indicating a potential positive role of 17α-estradiol treatment in male reproductive system. The elevated TFs such as *Sf1*, *Pparg*, *Litaf*, *Nupr1*, *Rxrg*, *E2f2*, and *Zfp42* may be involved in the transcriptional regulation by 17α-estradiol in O.T (**Figure 6D**). Importantly, the activities of androgen and estrogen pathways were decreased in *Gnrh1* neurons in O.T compared to O, and were distinct from those in *Ar*, *Esr1*, and *Esr2* neurons (**Figure 6E**). These signaling pathways are important for the feedback control of sex hormone secretion in *Gnrh* neurons, and these results may also reflect the strong effect of 17α-estradiol on *Gnrh* neurons.

To decipher the potential effects of elevated serum Gnrh levels on endocrine system, we performed bidirectional MR analysis of the GWAS summary data of human GNRH1 (id: prot-a-1233) and 203 endocrine-related factors with genetic variants SNPs. We found strong causal effects of GNRH1 on GAL/Galanin (id:prot−a−1166), POMC/Beta−endorphin (id:prot−a−2327, id:prot−a−2325), Adrenomedullin (id:prot−a−48), BDNF (id:prot−a−242**),** and LPR (id:prot−a−1724), which are involved in feeding, energy homeostasis, osmotic regulation, and neuron plasticity (**Figure 6F**). Notably, CRH/Corticotropin (id:prot−a−2326), PRLH/Prolactin−releasing peptide (id:prot−a−2376), NPW/Neuropeptide W (id:prot−a−2082), Glucagon (id:prot−a−1181), Chromogranin−A (id:prot−a−538) displayed bidirectional significance, indicating close and complex causal effects between GNRH1 and these endocrine factors (**Figure 6G, Figure 6—figure supplement 1A, B**). These results also suggest that the role of 17α-estradiol treatment in feeding, energy homeostasis, reproduction, osmotic regulation, stress response, and neuronal plasticity may be mediated, at least in part, by elevated Gnrh secretion.

Discussion

The most striking role of 17α-estradiol treatment revealed in this study showed that HPG axis was substantially improved in the levels of serum Gnrh and testosterone. The underlying molecular mechanism remains unclear; however, prior reports have indicated that 17α-estradiol can bind to ESR1 [9]. In our findings, 17α-estradiol treatment significantly decreased serum estradiol levels while elevating serum testosterone. Based on this evidence, we propose that 17α-estradiol may function similarly to estrogen receptor antagonists or aromatase inhibitors, potentially preventing the conversion of androgens to estrogens [28, 29]. These actions could alleviate the feedback

inhibition exerted by estrogen on hypothalamus and pituitary, thereby facilitating the secretion of Gnrh, FSH, and LH [30].

The testosterone levels in men gradually decline beginning in the third decade of life [31]. Age-related deterioration of the gonadotropic axis, particularly in older males with low serum testosterone, is often linked to numerous aging symptoms, including loss of skeletal muscle mass, reduced muscle strength and power, low bone mineral density, frailty, impaired physical performance, mobility limitations, increased risk of diabetes, elevated all-cause cardiovascular mortality, cognitive decline, and heightened risk of Alzheimer's disease [32]. Consequently, testosterone supplementation in older men is beneficial. Additionally, Gnrh supplementation may help mitigate age-related declines in neurogenesis and slow aging processes [33]. Importantly, treatment with 17α-estradiol did not result in feminization or adversely affect the sperm parameters and fertility in male animals [6, 14]. Thus, the observed increases in Gnrh and serum testosterone levels due to 17α-estradiol treatment are likely advantageous for older males, particularly those experiencing late-onset hypogonadism.

Postmenopausal women with low estrogen experience aging-related syndromes similar to those of older males with low serum testosterone. Those women also face increased mortality, cardiovascular disease, osteoporosis fracture, urogenital atrophy, and dementia, all of which may benefit from hormone therapy [34]. However, a prior report indicates that 17α-estradiol treatment does not provide positive life extension effects in aged females [13]. The discrepancy may stem from the inhibitory effects of estrogens associated with 17α-estradiol treatment, as evidenced by its inability to enhance female fertility [35]. Nonetheless, due to the lack of parallel data in aged female BN rats treated with 17α-estradiol, further research is needed to definitely address this question in the female subjects in the future.

Another notable effect of 17α-estradiol is its ability to reduce the overall expression levels of energy metabolism in hypothalamic neurons of aged male BN rats. The nutrient-sensing network, mediated by MTORC1 complex, is a central regulator of mRNA and ribosome biogenesis, protein synthesis, glucose metabolism, autophagy, lipid metabolism, mitochondrial biosynthesis, and proteasomal activity [36]. Downregulation of this nutrient-sensing network has been associated with increased lifespan and healthspan [37]. Notably, 17α-estradiol treatment diminished nutrient-sensing network activity in most hypothalamic neurons, which may be a contributing

factor in promoting lifespan extension.

In this report, we demonstrated significant changes in neuron populations involved in appetite control, including *Agrp*, *Pomc*, *Oxt*, *Oxtr*, *Gipr*, and *Glp2r* neurons. Among the identified subtypes, the proportion of Oxt neurons saw the most considerable increase due to 17α-estradiol treatment (**Figure 5A**). Oxt plays versatile roles in social behavior, stress response, satiety, energy balance, reproduction, and inflammation [38]. Most *Oxt* neurons originate from the paraventricular nucleus (PVN) and supraoptic nuclei (SON) in the hypothalamus, exhibiting high plasticity during development and intricate circuitry [39, 40]. The PVN, arcuate nucleus (ARC), and ventromedial hypothalamic nucleus together form a neural hub in the hypothalamus that integrates peripheral, nutritional, and metabolic signals to regulate food intake and energy balance [41]. Many effects of Oxt are sex-specific [42]; for instance, females are less sensitive to exogenous Oxt than males regarding social recognition [43]. Interestingly, Oxt injections, facilitated by nanoparticles that enhance blood-brain barrier penetration, reduced body mass while increasing social investigation and the number of Oxt-positive cells in the SON, particularly in male rats [44]. Additionally, intracerebroventricular injections of Oxt in rats showed a reduction in food intake in both sexes, with a more pronounced effect in males [45].Therefore, we propose that Oxt's role in systemic aging and feeding behavior may contribute to the sex-biased effects of 17α-estradiol, warranting further verification.

Furthermore, 17α-estradiol treatment appears to have enhanced stress in HPA axis. One evidence was the increased levels of ferroptosis-signature and UPR in *Crh* neurons. The other evidence was the elevated serum cortisol, which is also a potential hallmark of aging HPA axis [46, 47]. Therefore, more attentions should be paid to the potential side effects of 17α-estradiol especially in its clinical application.

In summary, our findings suggest that 17α-estradiol treatment positively influences the HPG axis and neurons associated with appetite and energy balance. This may be closely linked to the life-extension effects of 17α-estradiol in aged males. Additionally, employing supervised clustering based on neuropeptides, hormones, and their receptors proves to be a valuable strategy for examining pharmacological, pathological, and physiological processes in different neuronal subtypes within the hypothalamus.

Abbreviations

Ar: androgen receptor; ARC: arcuate nucleus; Astro: astrocyte; AUC: area under the curve; Cga: glycoprotein hormones, alpha Polypeptide; Crh: corticotropin releasing hormone; DEG: differentially-expressed gene; Endo: endothelial cell; Esr1: estrogen receptor 1; Esr2: estrogen receptor 2; Fibro: fibroblast; Glp2r: glucagon-like peptide 2 receptor; GnRH: gonadotropin releasing hormone; GSEA: gene set enrichment analysis; HPA: hypothalamic–pituitary–adrenal; HPG: hypothalamic-pituitary-gonadal; IEU: MRC Integrative Epidemiology Unit; IVW: inverse-variance weighting; KEGG: Kyoto Encyclopedia of Genes and Genomes; Micro: microglia; MR: Mendelian randomization; MTORC1: mechanistic target of rapamycin kinase 1; Nppa: natriuretic peptide A; Oligo: oligodendrocyte; OPC: oligodendrocyte precursor cell; OR: odds ratio; OXPHOS: oxidative phosphorylation; PID: Pathway Interaction Database; POMC: proopiomelanocortin; pQTL: protein quantitative trait loci; PTC: pars tuberalis cell; PVN: paraventricular nucleus; ROC: receiver operating characteristics; snRNA-seq: single-nucleus transcriptomic sequencing; Tany: tanycyte; TF: transcription factor; UPR: unfolded protein response.

Acknowledgments

We appreciate Dr. Qinghua Wang and Hongyun Shi from animal facility of Nantong University in helping with the animal experiments. Special thanks to Professor Ken-ichiro Fukuchi from University of Illinois College of Medicine for constructive comments and suggestions in manuscript preparation.

Funding: This work was supported by the National Natural Science Foundation of China grant 31271448 (YL), 82171621 (LL), 82172566 (ZY), 82150107 (RL) and the National High Level Hospital Clinical Research Funding (2022-PUMCH-A-231) (LL).

Author contributions: Conceptualization, YL, LL; Methodology, YL, GW, XX; Animal operation: YL, LL; EIA assays: YL, LY; Inflammation test: YL, ZY, LL, YS. Validation, LL, JY, ZY; Formal Analysis, YL, JY; Resources, GW, YS, ZY, ZM, LX; Visualization, YL; Writing – Original Draft, YL, JY; Writing – Review & Editing, LL, YS; Supervision, YS, ZY, YL; Project Administration, YL, ZY, LL; Funding Acquisition, ZY, LL. All authors have read and approved the final manuscript.

Declaration of competing interest

The authors have no conflict of interests to declare.

Availability of data and materials: All data are available at GEO accession number GSE248413.

Competing interests

All authors declare no competing interests.

References

1. Hajdarovic, K. H.; Yu, D.; Webb, A. E., Understanding the aging hypothalamus, one cell at a time. *Trends Neurosci* **2022,** 45, (12), 942-954.
2. Dacks, P. A.; Moreno, C. L.; Kim, E. S.; Marcellino, B. K.; Mobbs, C. V., Role of the hypothalamus in mediating protective effects of dietary restriction during aging. *Front Neuroendocrinol* **2013,** 34, (2), 95-106.
3. Masliukov, P. M., Changes of Signaling Pathways in Hypothalamic Neurons with Aging. *Curr Issues Mol Biol* **2023,** 45, (10), 8289-8308.
4. Yang, S. B.; Tien, A. C.; Boddupalli, G.; Xu, A. W.; Jan, Y. N.; Jan, L. Y., Rapamycin ameliorates age-dependent obesity associated with increased mTOR signaling in hypothalamic POMC neurons. *Neuron* **2012,** 75, (3), 425-36.
5. Yang, H.; Fang, B.; Wang, Z.; Chen, Y.; Dong, Y., The Timing Sequence and Mechanism of Aging in Endocrine Organs. *Cells* **2023,** 12, (7).
6. Stout, M. B.; Steyn, F. J.; Jurczak, M. J.; Camporez, J. G.; Zhu, Y.; Hawse, J. R.; Jurk, D.; Palmer, A. K.; Xu, M.; Pirtskhalava, T.; Evans, G. L.; de Souza Santos, R.; Frank, A. P.; White, T. A.; Monroe, D. G.; Singh, R. J.; Casaclang-Verzosa, G.; Miller, J. D.; Clegg, D. J.; LeBrasseur, N. K.; von Zglinicki, T.; Shulman, G. I.; Tchkonia, T.; Kirkland, J. L., 17α-Estradiol Alleviates Age-related Metabolic and Inflammatory Dysfunction in Male Mice Without Inducing Feminization. *J Gerontol A Biol Sci Med Sci* **2017,** 72, (1), 3-15.
7. Shen, Z.; Hinson, A.; Miller, R. A.; Garcia, G. G., Cap-independent translation: A shared mechanism for lifespan extension by rapamycin, acarbose, and 17α-estradiol. *Aging Cell* **2021,** 20, (5), e13345.
8. Wink, L.; Miller, R. A.; Garcia, G. G., Rapamycin, Acarbose and 17α-estradiol share common mechanisms regulating the MAPK pathways involved in intracellular signaling and inflammation. *Immun Ageing* **2022,** 19, (1), 8.
9. Mann, S. N.; Hadad, N.; Nelson Holte, M.; Rothman, A. R.; Sathiaseelan, R.; Ali Mondal, S.; Agbaga, M. P.; Unnikrishnan, A.; Subramaniam, M.; Hawse, J.; Huffman, D. M.; Freeman, W. M.; Stout, M. B., Health benefits attributed to 17α-estradiol, a lifespan-extending compound, are mediated through estrogen receptor α. *Elife* **2020,** 9.
10. Watanabe, K.; Wilmanski, T.; Baloni, P.; Robinson, M.; Garcia, G. G.; Hoopmann, M. R.; Midha, M. K.; Baxter, D. H.; Maes, M.; Morrone, S. R.; Crebs, K. M.; Kapil, C.; Kusebauch, U.; Wiedrick, J.; Lapidus, J.; Pflieger, L.; Lausted, C.; Roach, J. C.; Glusman, G.; Cummings, S. R.; Schork, N. J.; Price, N. D.; Hood, L.; Miller, R. A.; Moritz, R. L.; Rappaport, N., Lifespan-extending interventions induce consistent patterns of fatty acid oxidation in mouse livers. *Commun Biol* **2023,** 6, (1), 768.
11. Burns, A. R.; Wiedrick, J.; Feryn, A.; Maes, M.; Midha, M. K.; Baxter, D. H.; Morrone, S. R.;

Prokop, T. J.; Kapil, C.; Hoopmann, M. R.; Kusebauch, U.; Deutsch, E. W.; Rappaport, N.; Watanabe, K.; Moritz, R. L.; Miller, R. A.; Lapidus, J. A.; Orwoll, E. S., Proteomic changes induced by longevity-promoting interventions in mice. *Geroscience* **2024,** 46, (2), 1543-1560.

12. Steyn, F. J.; Ngo, S. T.; Chen, V. P.; Bailey-Downs, L. C.; Xie, T. Y.; Ghadami, M.; Brimijoin, S.; Freeman, W. M.; Rubinstein, M.; Low, M. J.; Stout, M. B., 17α-estradiol acts through hypothalamic pro-opiomelanocortin expressing neurons to reduce feeding behavior. *Aging Cell* **2018,** 17, (1).

13. Harrison, D. E.; Strong, R.; Allison, D. B.; Ames, B. N.; Astle, C. M.; Atamna, H.; Fernandez, E.; Flurkey, K.; Javors, M. A.; Nadon, N. L.; Nelson, J. F.; Pletcher, S.; Simpkins, J. W.; Smith, D.; Wilkinson, J. E.; Miller, R. A., Acarbose, 17-α-estradiol, and nordihydroguaiaretic acid extend mouse lifespan preferentially in males. *Aging Cell* **2014,** 13, (2), 273-82.

14. Isola, J. V. V.; Veiga, G. B.; de Brito, C. R. C.; Alvarado-Rincón, J. A.; Garcia, D. N.; Zanini, B. M.; Hense, J. D.; Vieira, A. D.; Garratt, M.; Gasperin, B. G.; Schneider, A.; Stout, M. B., 17α-estradiol does not adversely affect sperm parameters or fertility in male mice: implications for reproduction-longevity trade-offs. *Geroscience* **2023,** 45, (4), 2109-2120.

15. Stout, M. B.; Vaughan, K. L.; Isola, J. V. V.; Mann, S. N.; Wellman, B.; Hoffman, J. M.; Porter, H. L.; Freeman, W. M.; Mattison, J. A., Assessing tolerability and physiological responses to 17α-estradiol administration in male rhesus macaques. *Geroscience* **2023,** 45, (4), 2337-2349.

16. Harrison, D. E.; Strong, R.; Reifsnyder, P.; Kumar, N.; Fernandez, E.; Flurkey, K.; Javors, M. A.; Lopez-Cruzan, M.; Macchiarini, F.; Nelson, J. F.; Markewych, A.; Bitto, A.; Sindler, A. L.; Cortopassi, G.; Kavanagh, K.; Leng, L.; Bucala, R.; Rosenthal, N.; Salmon, A.; Stearns, T. M.; Bogue, M.; Miller, R. A., 17-a-estradiol late in life extends lifespan in aging UM-HET3 male mice; nicotinamide riboside and three other drugs do not affect lifespan in either sex. *Aging Cell* **2021,** 20, (5), e13328.

17. Strong, R.; Miller, R. A.; Antebi, A.; Astle, C. M.; Bogue, M.; Denzel, M. S.; Fernandez, E.; Flurkey, K.; Hamilton, K. L.; Lamming, D. W.; Javors, M. A.; de Magalhães, J. P.; Martinez, P. A.; McCord, J. M.; Miller, B. F.; Müller, M.; Nelson, J. F.; Ndukum, J.; Rainger, G. E.; Richardson, A.; Sabatini, D. M.; Salmon, A. B.; Simpkins, J. W.; Steegenga, W. T.; Nadon, N. L.; Harrison, D. E., Longer lifespan in male mice treated with a weakly estrogenic agonist, an antioxidant, an α-glucosidase inhibitor or a Nrf2-inducer. *Aging Cell* **2016,** 15, (5), 872-84.

18. Rath, S.; Sharma, R.; Gupta, R.; Ast, T.; Chan, C.; Durham, T. J.; Goodman, R. P.; Grabarek, Z.; Haas, M. E.; Hung, W. H. W.; Joshi, P. R.; Jourdain, A. A.; Kim, S. H.; Kotrys, A. V.; Lam, S. S.; McCoy, J. G.; Meisel, J. D.; Miranda, M.; Panda, A.; Patgiri, A.; Rogers, R.; Sadre, S.; Shah, H.; Skinner, O. S.; To, T. L.; Walker, M. A.; Wang, H.; Ward, P. S.; Wengrod, J.; Yuan, C. C.; Calvo, S. E.; Mootha, V. K., MitoCarta3.0: an updated mitochondrial proteome now with sub-organelle localization and pathway annotations. *Nucleic Acids Res* **2021,** 49, (D1), D1541-d1547.

19. Hu, H.; Miao, Y. R.; Jia, L. H.; Yu, Q. Y.; Zhang, Q.; Guo, A. Y., AnimalTFDB 3.0: a comprehensive resource for annotation and prediction of animal transcription factors. *Nucleic Acids Res* **2019,** 47, (D1), D33-d38.

20. Lu, H.; Ping, J.; Zhou, G.; Zhao, Z.; Gao, W.; Jiang, Y.; Quan, C.; Lu, Y.; Zhou, G., CommPath: An R package for inference and analysis of pathway-mediated cell-cell communication chain from single-cell transcriptomics. *Comput Struct Biotechnol J* **2022,** 20, 5978-5983.

21. Badia, I. M. P.; Vélez Santiago, J.; Braunger, J.; Geiss, C.; Dimitrov, D.; Müller-Dott, S.; Taus, P.; Dugourd, A.; Holland, C. H.; Ramirez Flores, R. O.; Saez-Rodriguez, J., decoupleR: ensemble of computational methods to infer biological activities from omics data. *Bioinform Adv* **2022,** 2, (1), vbac016.

22. Liao, Y.; Wang, J.; Jaehnig, E. J.; Shi, Z.; Zhang, B., WebGestalt 2019: gene set analysis toolkit with revamped UIs and APIs. *Nucleic Acids Res* **2019,** 47, (W1), W199-w205.

23. Hemani, G.; Zheng, J.; Elsworth, B.; Wade, K. H.; Haberland, V.; Baird, D.; Laurin, C.; Burgess, S.; Bowden, J.; Langdon, R.; Tan, V. Y.; Yarmolinsky, J.; Shihab, H. A.; Timpson, N. J.; Evans, D. M.; Relton, C.; Martin, R. M.; Davey Smith, G.; Gaunt, T. R.; Haycock, P. C., The MR-Base platform supports systematic causal inference across the human phenome. *Elife* **2018,** 7.

24. Sun, B. B.; Maranville, J. C.; Peters, J. E.; Stacey, D.; Staley, J. R.; Blackshaw, J.; Burgess, S.; Jiang, T.; Paige, E.; Surendran, P.; Oliver-Williams, C.; Kamat, M. A.; Prins, B. P.; Wilcox, S. K.; Zimmerman, E. S.; Chi, A.; Bansal, N.; Spain, S. L.; Wood, A. M.; Morrell, N. W.; Bradley, J. R.; Janjic, N.; Roberts, D. J.; Ouwehand, W. H.; Todd, J. A.; Soranzo, N.; Suhre, K.; Paul, D. S.; Fox, C. S.; Plenge, R. M.; Danesh, J.; Runz, H.; Butterworth, A. S., Genomic atlas of the human plasma proteome. *Nature* **2018,** 558, (7708), 73-79.

25. Hemani, G.; Tilling, K.; Davey Smith, G., Orienting the causal relationship between imprecisely measured traits using GWAS summary data. *PLoS Genet* **2017,** 13, (11), e1007081.

26. Inada, K.; Tsujimoto, K.; Yoshida, M.; Nishimori, K.; Miyamichi, K., Oxytocin signaling in the posterior hypothalamus prevents hyperphagic obesity in mice. *Elife* **2022,** 11.

27. Dalvi, P. S.; Belsham, D. D., Glucagon-like peptide-2 directly regulates hypothalamic neurons expressing neuropeptides linked to appetite control in vivo and in vitro. *Endocrinology* **2012,** 153, (5), 2385-97.

28. Leder, B. Z.; Rohrer, J. L.; Rubin, S. D.; Gallo, J.; Longcope, C., Effects of aromatase inhibition in elderly men with low or borderline-low serum testosterone levels. *J Clin Endocrinol Metab* **2004,** 89, (3), 1174-80.

29. Guay, A. T.; Jacobson, J.; Perez, J. B.; Hodge, M. B.; Velasquez, E., Clomiphene increases free testosterone levels in men with both secondary hypogonadism and erectile dysfunction: who does and does not benefit? *Int J Impot Res* **2003,** 15, (3), 156-65.

30. Wang, C.; Swerdloff, R. S., Testosterone Replacement Therapy in Hypogonadal Men. *Endocrinol Metab Clin North Am* **2022,** 51, (1), 77-98.

31. Camacho, E. M.; Huhtaniemi, I. T.; O'Neill, T. W.; Finn, J. D.; Pye, S. R.; Lee, D. M.; Tajar, A.; Bartfai, G.; Boonen, S.; Casanueva, F. F.; Forti, G.; Giwercman, A.; Han, T. S.; Kula, K.; Keevil, B.; Lean, M. E.; Pendleton, N.; Punab, M.; Vanderschueren, D.; Wu, F. C., Age-associated changes in hypothalamic-pituitary-testicular function in middle-aged and older men are modified by weight change and lifestyle factors: longitudinal results from the European Male Ageing Study. *Eur J Endocrinol* **2013,** 168, (3), 445-55.

32. Rodrigues Dos Santos, M.; Bhasin, S., Benefits and Risks of Testosterone Treatment in Men with Age-Related Decline in Testosterone. *Annu Rev Med* **2021,** 72, 75-91.

33. Zhang, G.; Li, J.; Purkayastha, S.; Tang, Y.; Zhang, H.; Yin, Y.; Li, B.; Liu, G.; Cai, D., Hypothalamic programming of systemic ageing involving IKK-β, NF-κB and GnRH. *Nature* **2013,** 497, (7448), 211-6.

34. Shoupe, D., Individualizing hormone therapy to minimize risk: accurate assessment of risks and benefits. *Womens Health (Lond)* **2011,** 7, (4), 475-85.
35. Isola, J. V. V.; Zanini, B. M.; Hense, J. D.; Alvarado-Rincón, J. A.; Garcia, D. N.; Pereira, G. C.; Vieira, A. D.; Oliveira, T. L.; Collares, T.; Gasperin, B. G.; Stout, M. B.; Schneider, A., Mild calorie restriction, but not 17α-estradiol, extends ovarian reserve and fertility in female mice. *Exp Gerontol* **2022,** 159, 111669.
36. López-Otín, C.; Blasco, M. A.; Partridge, L.; Serrano, M.; Kroemer, G., Hallmarks of aging: An expanding universe. *Cell* **2023,** 186, (2), 243-278.
37. Singh, P. P.; Demmitt, B. A.; Nath, R. D.; Brunet, A., The Genetics of Aging: A Vertebrate Perspective. *Cell* **2019,** 177, (1), 200-220.
38. Kerem, L.; Lawson, E. A., The Effects of Oxytocin on Appetite Regulation, Food Intake and Metabolism in Humans. *Int J Mol Sci* **2021,** 22, (14).
39. Rosen, G. J.; de Vries, G. J.; Goldman, S. L.; Goldman, B. D.; Forger, N. G., Distribution of oxytocin in the brain of a eusocial rodent. *Neuroscience* **2008,** 155, (3), 809-17.
40. Madrigal, M. P.; Jurado, S., Specification of oxytocinergic and vasopressinergic circuits in the developing mouse brain. *Commun Biol* **2021,** 4, (1), 586.
41. Cornejo, M. P.; Hentges, S. T.; Maliqueo, M.; Coirini, H.; Becu-Villalobos, D.; Elias, C. F., Neuroendocrine Regulation of Metabolism. *J Neuroendocrinol* **2016,** 28, (7).
42. Carvalho Silva, R.; Pisanu, C.; Maffioletti, E.; Menesello, V.; Bortolomasi, M.; Gennarelli, M.; Baune, B. T.; Squassina, A.; Minelli, A., Biological markers of sex-based differences in major depressive disorder and in antidepressant response. *Eur Neuropsychopharmacol* **2023,** 76, 89-107.
43. Dumais, K. M.; Veenema, A. H., Vasopressin and oxytocin receptor systems in the brain: Sex differences and sex-specific regulation of social behavior. *Front Neuroendocrinol* **2016,** 40, 1-23.
44. Duarte-Guterman, P.; Lieblich, S. E.; Qiu, W.; Splinter, J. E. J.; Go, K. A.; Casanueva-Reimon, L.; Galea, L. A. M., Oxytocin has sex-specific effects on social behaviour and hypothalamic oxytocin immunoreactive cells but not hippocampal neurogenesis in adult rats. *Horm Behav* **2020,** 122, 104734.
45. Liu, C. M.; Davis, E. A.; Suarez, A. N.; Wood, R. I.; Noble, E. E.; Kanoski, S. E., Sex Differences and Estrous Influences on Oxytocin Control of Food Intake. *Neuroscience* **2020,** 447, 63-73.
46. Veldhuis, J. D., Changes in pituitary function with ageing and implications for patient care. *Nat Rev Endocrinol* **2013,** 9, (4), 205-15.
47. Warde, K. M.; Smith, L. J.; Basham, K. J., Age-related Changes in the Adrenal Cortex: Insights and Implications. *J Endocr Soc* **2023,** 7, (9), bvad097.

Figure legends

Figure 1. snRNA-seq profiling of the hypothalamus from O, O.T and Y samples. (A) UMAP visualization of nuclei colored by 10 cell types: neuron (Neu), astrocyte (Astro), oligodendrocyte (Oligo), oligodendrocyte precursor cell (OPC), tanycyte (Tany), ependymocyte (Epen), microglia (Micro), fibroblast (Fibro), pars tuberalis cell (PTC), and endothelial cell (Endo), from

hypothalamus of aged rats (O), 17α-estradiol-treated aged rats (O.T) and young rats (Y). **(B)** Heatmap showing the classic markers of 10 major cell types in hypothalamus. **(C)** Cell-type compositions by groups (left panel) or by major cell types with the total cell numbers shown above each column. **(D)** Circos plot depicting the number of ligand–receptor pairs between Neu and other cell types (color strips) for each group. **(E)** Dot plot showing significant ligand–receptor interactions between Neurons for each group. Boxes showing the unique ligand–receptor interactions between Neuron.O (black boxes) or between Neuron.O.T (blue boxes). **(F)** Dot plot of the top 6 enriched GO biological process terms across three groups of neurons via GSEA analysis. **(G)** The top 15 changed pathways/gene sets according to the ranks of AUC values in selected pathways related to neuronal synapses and axons from Gene Ontology (GO) biological process, GO molecular function and GO cellular component.

Figure 2. Two opposing regulatory signaling networks in neuron metabolism. (A) Dot plot of the selected pathways representing the prominent changes of overall expression levels across Neuron.O, Neuron.O.T and Neuron.Y in metabolism, signaling and synaptic activity. **(B)** Correlation heatmap showing transcription factors (TFs) that correlated with the two opposing regulatory signaling networks in the mixed neurons of O, O.T and Y. **(C)** The shared unique markers of each quarter (c1-c4) in 6 pathways in hypothalamic neurons (O, O.T, and Y). The markers were then collected as c1.up.signature (19 genes) and c4.up.signature (12 genes). **(D)** The aging-related cell proportions of each quarter shown by 4 pathways. **(E)** The correlation of c1.up.signature and c2.up.signature with the two opposing regulatory signaling networks.

Figure 3. Screening of neuron subtypes by supervised clustering that responded distinctly to aging and 17α-estradiol treatment. (A) Diagram outlining the features of supervised clustering of neurons in hypothalamus compared with the traditional unsupervised clustering. **(B)** The top 10 and bottom 10 neurons of 121 neurons according to the mean expression values of eight signaling pathways from stress, apoptosis, metabolism, immune response, and senescence in Neuron.O. The expression levels of these neuron subtypes from Neuron.O.T and Neuron.Y were also indicated. **(C)** Word clouds displaying the frequency of neurons that were among the top 10 in each of the 16 signaling pathways as shown in **Table S2**. The 16 pathways were from oxidative stress, apoptosis,

metabolism, immune response, and senescence. **(D)** Venn diagram showing the number of neuron subtypes exclusively in each group or shared by the groups in (C). The neurons with frequency >3 were selected for calculation in (C). **(E)** The top 15 and bottom 15 neurons among 121 neurons according to the mean expression levels of c1.up.signature and c4.up.signature in Neuron.O. **(F)** The top 15 and bottom 15 neurons among 121 neurons according to the mean expression levels of c1.up.signature and c4.up.signature in Neuron.O.T.

Figure 4. The responses of Crh neurons to long-term 17α-estradiol treatment. (A) The two intersected neurons among the top 10 neurons according to the mean expression levels of the three senescence-related pathways. **(B)** The expression profiles of selected pathways from the two opposing signaling networks in Neuron *Crh*, *Nppa* and *Nppc*. Neuron *Crh* and *Nppa* were the only two types of neurons shared by the three top 10 neurons in (A). **(C)** The downregulated and upregulated DEGs expressed by mitochondria or in pathway adherens junction between O.T and O in Crh neurons. **(D)** The top 25 TF activities in *Crh* and *Gnrh1* neurons. **(E)** Enzyme immunoassay of the serum levels of Crh, cortisol, and aldosterone in Y, O and O.T. Two-tail unpaired T-test was performed. p values were labeled.

Figure 5. The response of Oxt neurons to 17α-estradiol and the causal effects of Oxt on other endocrine factors.

(A), (B) The top 10 (arrows) and bottom 10 (arrows) types of neurons from 121 subtypes ranked in cell proportions among three groups. **(C)** Dot plots showing the expression profiles of the selected pathways from the two opposing signaling pathways in four types of food uptake-related neurons, which decreased or increased among the top 10 ranks in (A) or (B). Blue arrows: c1.up.signature and c4.up.signature. **(D)** Volcanic plots showing the DEGs between Neuron.O.T and Neuron.O in the pathway synaptic membrane. **(E)** Enzyme immunoassay of the plasma levels of Oxt in three groups. **(F)** Top 25 TF activities in neuron Oxt. **(G)** Significant causal effects ($p < 0.05$, IVW) between exposure OXT (id: prot-a-2159) and 203 endocrine-related outcomes, which were not significant in reverse MR analysis. Significant heterogeneity (Q_pval < 0.05). Significant horizontal pleiotropy (pval < 0.05).

Figure 6. The response of HPG axis in the males to 17α-estradiol and the causal effects of Gnrh on other endocrine factors. (A) The expression profiles of pathways from the two opposing signaling networks in Gnrh1-, Esr2-, Esr1- or Ar-positive neurons. **(B)** Enzyme immunoassay of the serum levels of Gnrh, total testosterone (T), and estrogen (E) in Y, O and O.T samples. Two-tail unpaired T-test was performed. **(C)** Inflammation of seminiferous tubules in testes of O and O.T. Left two panels: representative HE staining of testis inflammation in O and the normal seminiferous tubules of O.T. Right panel: the mean testis inflammation index of O and O.T. **(D)** The top 25 TF activities in Gnrh1 neurons in three groups. **(E)** The activities of 14 pathways in Gnrh1-, Esr2-, Esr1- or Ar-positive neurons. **(F)** Significant causal effects (IVW, $p < 0.05$) between exposure GNRH1 (id: prot-a-1233) and 203 endocrine-related outcomes, which were not significant in reverse MR analysis. **(G)** Items with significant causal effects (IVW, $p < 0.05$) in both directions of MR analysis between GNRH1 (id: prot-a-1233) and 203 endocrine-related outcomes.

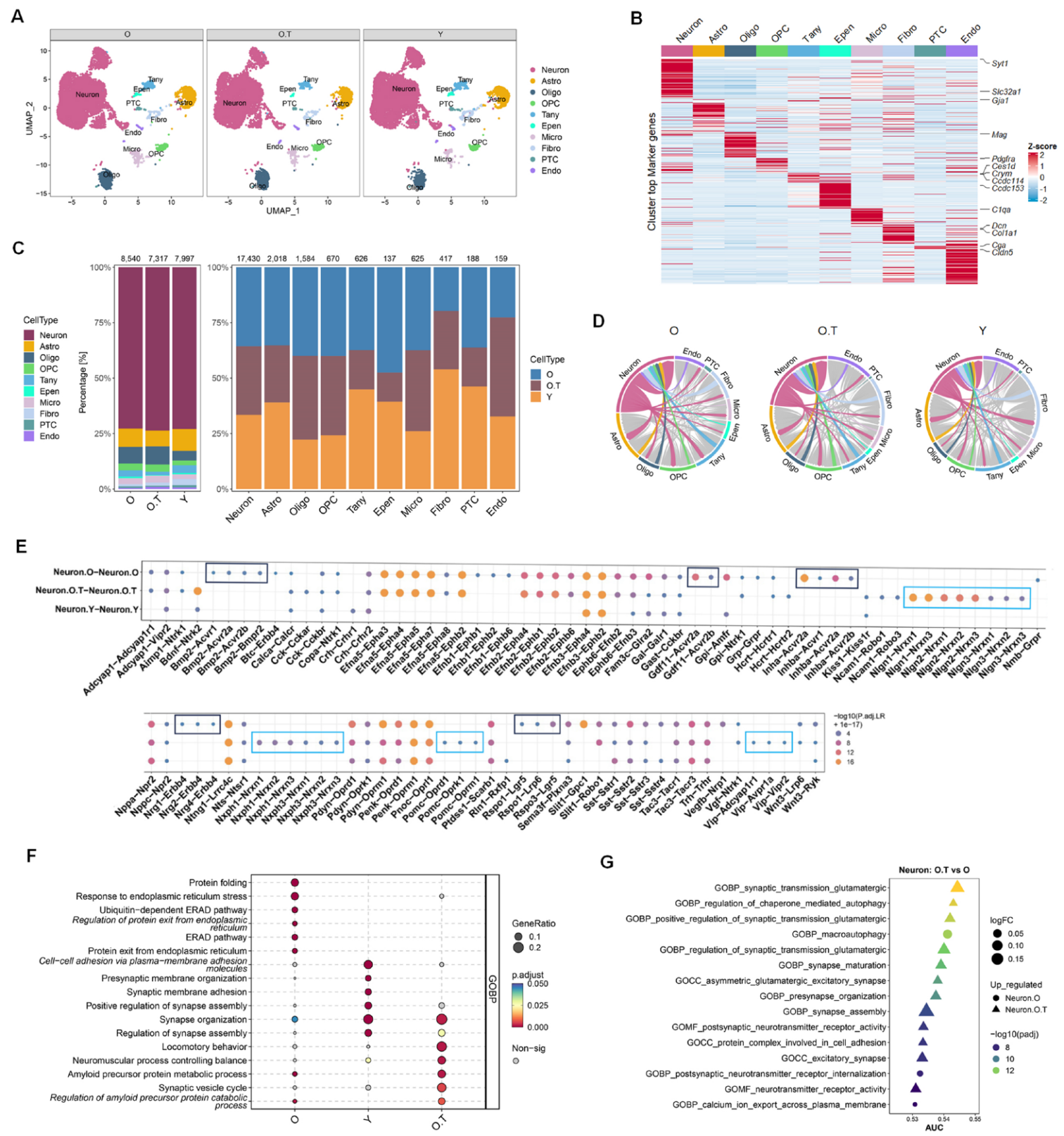
A
O
O.T
Y
UMAP_1
UMAP_2
Neuron
Astro
Oligo
OPC
Tany
Epen
Micro
Fibro
PTC
Endo
B
Cluster top Marker genes
Z-score
Syt1
Slc32a1
Gja1
Mag
Pdgfra
Ces1d
Crym
Ccdc114
Ccdc153
C1qa
Dcn
Col1a1
Cga
Cldn5
C
CellType
Percentage [%]
8,540
7,317
7,997
17,430
2,018
1,584
670
626
137
625
417
188
159
D
E
Neuron.O−Neuron.O
Neuron.O.T−Neuron.O.T
Neuron.Y−Neuron.Y
−log10(P.adj.LR + 1e−17)
F
Protein folding
Response to endoplasmic reticulum stress
Ubiquitin−dependent ERAD pathway
Regulation of protein exit from endoplasmic reticulum
ERAD pathway
Protein exit from endoplasmic reticulum
Cell−cell adhesion via plasma−membrane adhesion molecules
Presynaptic membrane organization
Synaptic membrane adhesion
Positive regulation of synapse assembly
Synapse organization
Regulation of synapse assembly
Locomotory behavior
Neuromuscular process controlling balance
Amyloid precursor protein metabolic process
Synaptic vesicle cycle
Regulation of amyloid precursor protein catabolic process
GeneRatio
p.adjust
Non−sig
GOBP
G
Neuron: O.T vs O
GOBP_synaptic_transmission_glutamatergic
GOBP_regulation_of_chaperone_mediated_autophagy
GOBP_positive_regulation_of_synaptic_transmission_glutamatergic
GOBP_macroautophagy
GOBP_regulation_of_synaptic_transmission_glutamatergic
GOBP_synapse_maturation
GOCC_asymmetric_glutamatergic_excitatory_synapse
GOBP_presynapse_organization
GOBP_synapse_assembly
GOMF_postsynaptic_neurotransmitter_receptor_activity
GOCC_protein_complex_involved_in_cell_adhesion
GOCC_excitatory_synapse
GOBP_postsynaptic_neurotransmitter_receptor_internalization
GOMF_neurotransmitter_receptor_activity
GOBP_calcium_ion_export_across_plasma_membrane
logFC
Up_regulated
Neuron.O
Neuron.O.T
−log10(padj)
AUC

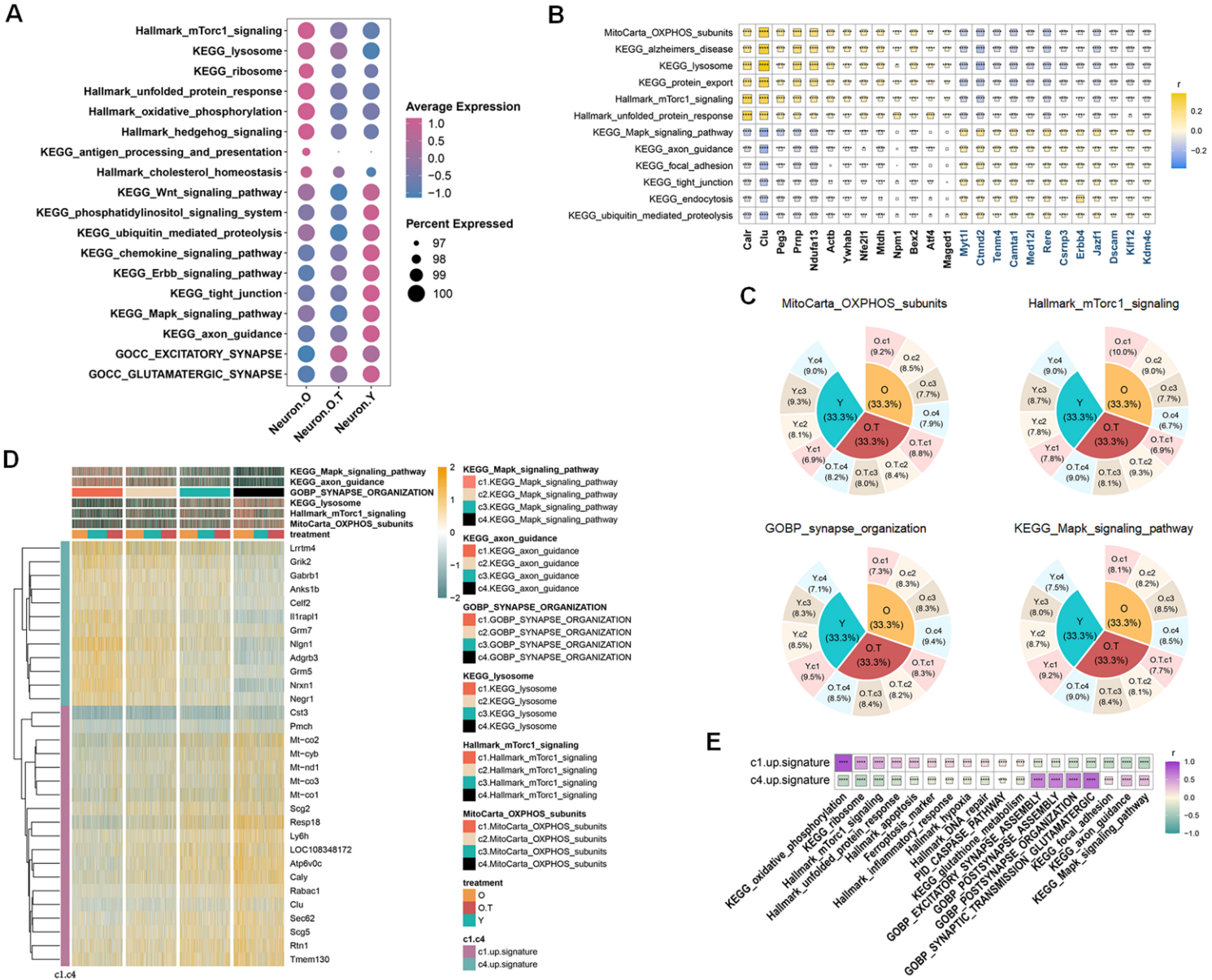
A
Hallmark_mTorc1_signaling
KEGG_lysosome
KEGG_ribosome
Hallmark_unfolded_protein_response
Hallmark_oxidative_phosphorylation
Hallmark_hedgehog_signaling
KEGG_antigen_processing_and_presentation
Hallmark_cholesterol_homeostasis
KEGG_Wnt_signaling_pathway
KEGG_phosphatidylinositol_signaling_system
KEGG_ubiquitin_mediated_proteolysis
KEGG_chemokine_signaling_pathway
KEGG_Erbb_signaling_pathway
KEGG_tight_junction
KEGG_Mapk_signaling_pathway
KEGG_axon_guidance
GOCC_EXCITATORY_SYNAPSE
GOCC_GLUTAMATERGIC_SYNAPSE
Neuron.O
Neuron.O.T
Neuron.Y
Average Expression
1.0
0.5
0.0
−0.5
−1.0
Percent Expressed
97
98
99
100
B
MitoCarta_OXPHOS_subunits
KEGG_alzheimers_disease
KEGG_lysosome
KEGG_protein_export
Hallmark_mTorc1_signaling
Hallmark_unfolded_protein_response
KEGG_Mapk_signaling_pathway
KEGG_axon_guidance
KEGG_focal_adhesion
KEGG_tight_junction
KEGG_endocytosis
KEGG_ubiquitin_mediated_proteolysis
Calr
Clu
Peg3
Prnp
Ndufa13
Actb
Ywhab
Nfe2l1
Mtdh
Npm1
Bex2
Atf4
Maged1
Myt1l
Ctnnd2
Tenm4
Camta1
Med12l
Rere
Csrnp3
Erbb4
Jazf1
Dscam
Klf12
Kdm4c
r
0.2
0.0
−0.2
C
MitoCarta_OXPHOS_subunits
Hallmark_mTorc1_signaling
GOBP_synapse_organization
KEGG_Mapk_signaling_pathway
O
(33.3%)
O.T
(33.3%)
Y
(33.3%)
O.c1 (9.2%)
O.c2 (8.5%)
O.c3 (7.7%)
O.c4 (7.9%)
O.T.c1 (8.8%)
O.T.c2 (8.4%)
O.T.c3 (8.0%)
O.T.c4 (8.2%)
Y.c1 (6.9%)
Y.c2 (8.1%)
Y.c3 (9.3%)
Y.c4 (9.0%)
O.c1 (10.0%)
O.c2 (9.0%)
O.c3 (7.7%)
O.c4 (6.7%)
O.T.c1 (6.9%)
O.T.c2 (9.3%)
O.T.c3 (8.1%)
O.T.c4 (9.0%)
Y.c1 (7.8%)
Y.c2 (7.8%)
Y.c3 (8.7%)
Y.c4 (9.0%)
O.c1 (7.3%)
O.c2 (8.3%)
O.c3 (8.3%)
O.c4 (9.4%)
O.T.c1 (8.3%)
O.T.c2 (8.2%)
O.T.c3 (8.4%)
O.T.c4 (8.5%)
Y.c1 (9.5%)
Y.c2 (8.5%)
Y.c3 (8.3%)
Y.c4 (7.1%)
O.c1 (8.1%)
O.c2 (8.2%)
O.c3 (8.5%)
O.c4 (8.5%)
O.T.c1 (7.7%)
O.T.c2 (8.1%)
O.T.c3 (8.4%)
O.T.c4 (9.0%)
Y.c1 (9.2%)
Y.c2 (8.7%)
Y.c3 (8.0%)
Y.c4 (7.5%)
D
KEGG_Mapk_signaling_pathway
KEGG_axon_guidance
GOBP_SYNAPSE_ORGANIZATION
KEGG_lysosome
Hallmark_mTorc1_signaling
MitoCarta_OXPHOS_subunits
treatment
Lrrtm4
Grik2
Gabrb1
Anks1b
Celf2
Il1rapl1
Grm7
Nlgn1
Adgrb3
Grm5
Nrxn1
Negr1
Cst3
Pmch
Mt−co2
Mt−cyb
Mt−nd1
Mt−co3
Mt−co1
Scg2
Resp18
Ly6h
LOC108348172
Atp6v0c
Caly
Rabac1
Clu
Sec62
Scg5
Rtn1
Tmem130
c1.c4
2
1
0
−1
−2
KEGG_Mapk_signaling_pathway
c1.KEGG_Mapk_signaling_pathway
c2.KEGG_Mapk_signaling_pathway
c3.KEGG_Mapk_signaling_pathway
c4.KEGG_Mapk_signaling_pathway
KEGG_axon_guidance
c1.KEGG_axon_guidance
c2.KEGG_axon_guidance
c3.KEGG_axon_guidance
c4.KEGG_axon_guidance
GOBP_SYNAPSE_ORGANIZATION
c1.GOBP_SYNAPSE_ORGANIZATION
c2.GOBP_SYNAPSE_ORGANIZATION
c3.GOBP_SYNAPSE_ORGANIZATION
c4.GOBP_SYNAPSE_ORGANIZATION
KEGG_lysosome
c1.KEGG_lysosome
c2.KEGG_lysosome
c3.KEGG_lysosome
c4.KEGG_lysosome
Hallmark_mTorc1_signaling
c1.Hallmark_mTorc1_signaling
c2.Hallmark_mTorc1_signaling
c3.Hallmark_mTorc1_signaling
c4.Hallmark_mTorc1_signaling
MitoCarta_OXPHOS_subunits
c1.MitoCarta_OXPHOS_subunits
c2.MitoCarta_OXPHOS_subunits
c3.MitoCarta_OXPHOS_subunits
c4.MitoCarta_OXPHOS_subunits
treatment
O
O.T
Y
c1.c4
c1.up.signature
c4.up.signature
E
c1.up.signature
c4.up.signature
KEGG_oxidative_phosphorylation
KEGG_ribosome
Hallmark_mTorc1_signaling
Hallmark_unfolded_protein_response
Hallmark_apoptosis
Ferroptosis_marker
Hallmark_inflammatory_response
Hallmark_hypoxia
Hallmark_DNA_repair
PID_CASPASE_PATHWAY
KEGG_glutathione_metabolism
GOBP_EXCITATORY_SYNAPSE_ASSEMBLY
GOBP_POSTSYNAPSE_ASSEMBLY
GOBP_POSTSYNAPSE_ORGANIZATION
GOBP_SYNAPTIC_TRANSMISSION_GLUTAMATERGIC
KEGG_focal_adhesion
KEGG_axon_guidance
KEGG_Mapk_signaling_pathway
r
1.0
0.5
0.0
−0.5
−1.0

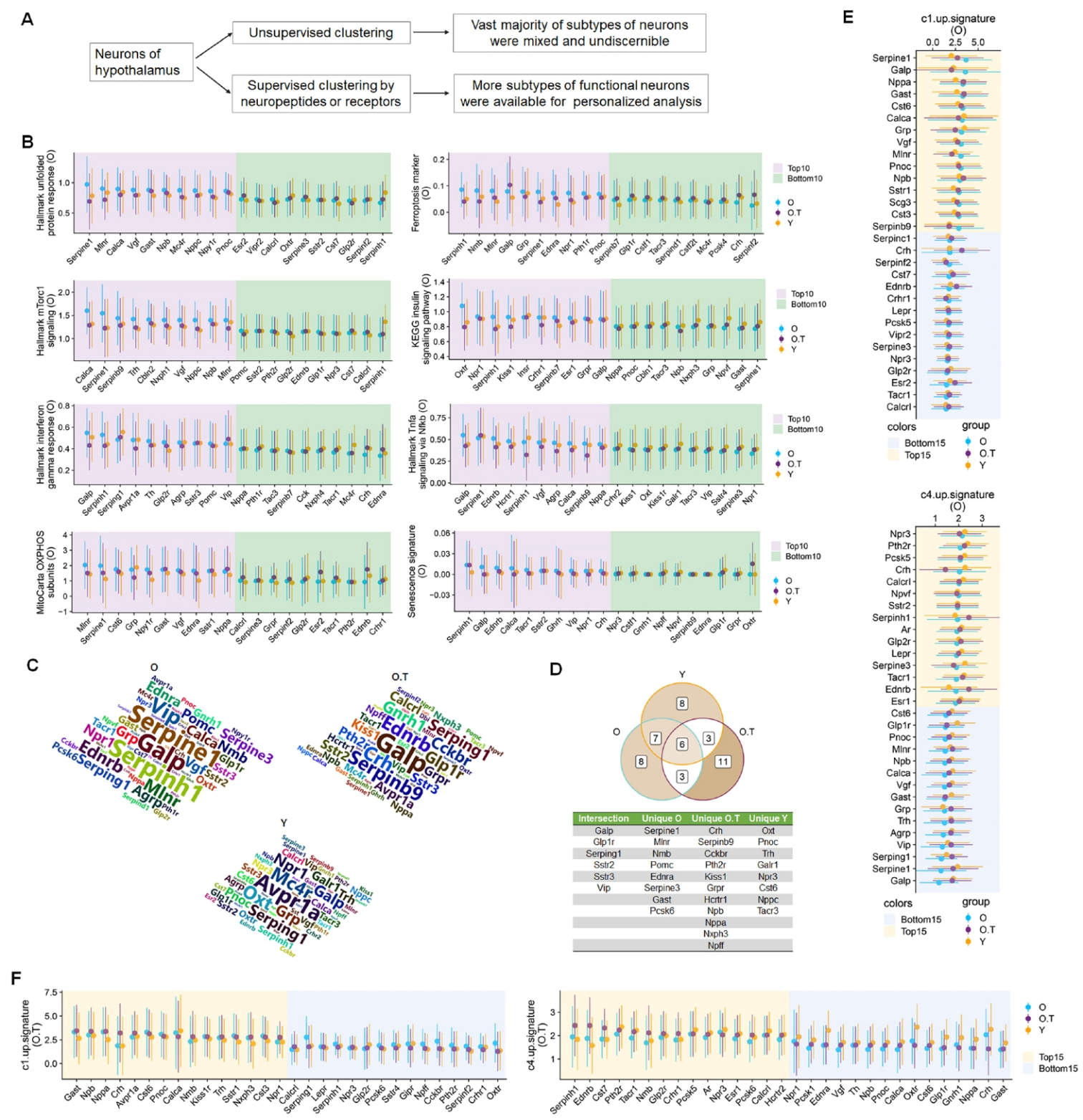
A
Neurons of hypothalamus
Unsupervised clustering
Vast majority of subtypes of neurons were mixed and undiscernible
Supervised clustering by neuropeptides or receptors
More subtypes of functional neurons were available for personalized analysis
B
Hallmark unfolded protein response (O)
Ferroptosis marker (O)
Hallmark mTorc1 signaling (O)
KEGG insulin signaling pathway (O)
Hallmark interferon gamma response (O)
Hallmark Tnfa signaling via Nfkb (O)
MitoCarta OXPHOS subunits (O)
Senescence signature (O)
Top10
Bottom10
O
O.T
Y
C
O
O.T
Y
D
Y
O
O.T
8
7
6
3
8
11
3
Intersection | Unique O | Unique O.T | Unique Y
Galp | Serpine1 | Crh | Oxt
Glp1r | Mlnr | Serpinb9 | Pnoc
Serping1 | Nmb | Cckbr | Trh
Sstr2 | Pomc | Pth2r | Galr1
Sstr3 | Ednra | Kiss1 | Npr3
Vip | Serpine3 | Grpr | Cst6
| Gast | Hcrtr1 | Nppc
| Pcsk6 | Npb | Tacr3
	Nppa
	Nxph3
	Npff
E
c1.up.signature (O)
c4.up.signature (O)
colors
group
Bottom15
Top15
O
O.T
Y
F
c1.up.signature (O.T)
c4.up.signature (O.T)
Top15
Bottom15

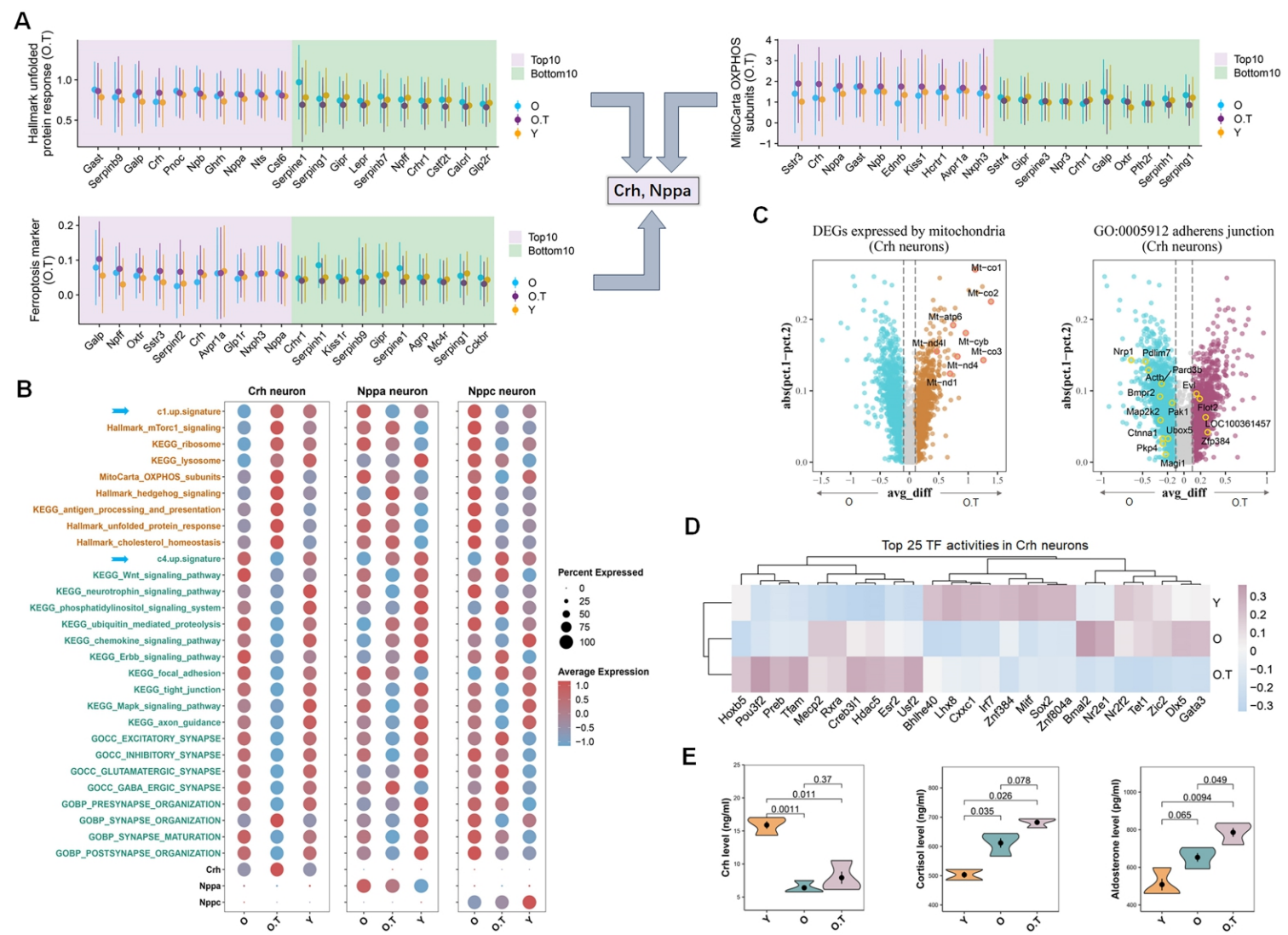
A
Hallmark unfolded protein response (O.T)
Top10
Bottom10
O
O.T
Y
Gast Serpinb9 Galp Crh Pnoc Npb Ghrh Nppa Nts Cst6 Serpine1 Serping1 Gipr Lepr Serpinb7 Npff Crhr1 Cstf2t Calcr1 Glp2r
MitoCarta OXPHOS subunits (O.T)
Sstr3 Crh Nppa Gast Npb Ednrb Kiss1 Hcrtr1 Avpr1a Nxph3 Sstr4 Gipr Serpine3 Npr3 Crhr1 Galp Oxtr Pth2r Serpinh1 Serping1
Ferroptosis marker (O.T)
Galp Npff Oxtr Sstr3 Serpinf2 Crh Avpr1a Glp1r Nxph3 Nppa Crhr1 Serpinh1 Kiss1r Serpinb9 Gipr Serpine1 Agrp Mc4r Serping1 Cckbr
Crh, Nppa
B
Crh neuron
Nppa neuron
Nppc neuron
c1.up.signature
Hallmark_mTorc1_signaling
KEGG_ribosome
KEGG_lysosome
MitoCarta_OXPHOS_subunits
Hallmark_hedgehog_signaling
KEGG_antigen_processing_and_presentation
Hallmark_unfolded_protein_response
Hallmark_cholesterol_homeostasis
c4.up.signature
KEGG_Wnt_signaling_pathway
KEGG_neurotrophin_signaling_pathway
KEGG_phosphatidylinositol_signaling_system
KEGG_ubiquitin_mediated_proteolysis
KEGG_chemokine_signaling_pathway
KEGG_Erbb_signaling_pathway
KEGG_focal_adhesion
KEGG_tight_junction
KEGG_Mapk_signaling_pathway
KEGG_axon_guidance
GOCC_EXCITATORY_SYNAPSE
GOCC_INHIBITORY_SYNAPSE
GOCC_GLUTAMATERGIC_SYNAPSE
GOCC_GABA_ERGIC_SYNAPSE
GOBP_PRESYNAPSE_ORGANIZATION
GOBP_SYNAPSE_ORGANIZATION
GOBP_SYNAPSE_MATURATION
GOBP_POSTSYNAPSE_ORGANIZATION
Crh
Nppa
Nppc
Percent Expressed
Average Expression
C
DEGs expressed by mitochondria (Crh neurons)
GO:0005912 adherens junction (Crh neurons)
abs(pct.1−pct.2)
avg_diff
Mt-co1
Mt-co2
Mt-atp6
Mt-nd4l
Mt-cyb
Mt-co3
Mt-nd4
Mt-nd1
Nrp1
Pdlim7
Pard3b
Actb
Evl
Bmpr2
Flot2
Map2k2
Pak1
LOC100361457
Ctnna1
Ubox5
Zfp384
Pkp4
Magi1
D
Top 25 TF activities in Crh neurons
Hoxb5 Pou3f2 Preb Tfam Mecp2 Rxra Creb3l1 Hdac5 Esr2 Usf2 Bhlhe40 Lhx8 Cxxc1 Irf7 Znf384 Mitf Sox2 Znf804a Bmal2 Nr2e1 Nr2f2 Tet1 Zic2 Dlx5 Gata3
E
Crh level (ng/ml)
Cortisol level (ng/ml)
Aldosterone level (pg/ml)
0.37
0.011
0.0011
0.078
0.026
0.035
0.049
0.0094
0.065

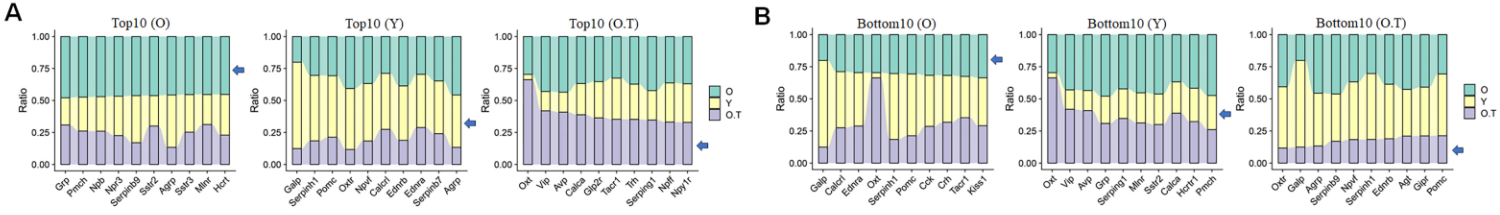

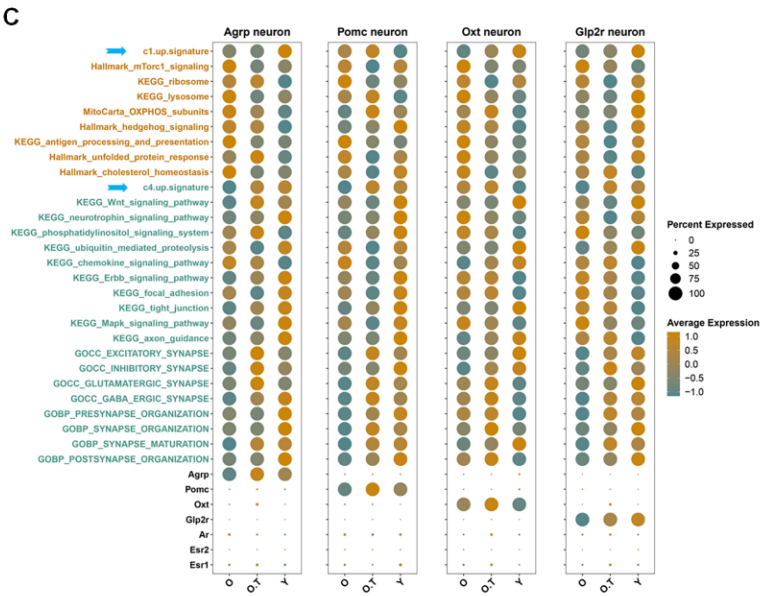

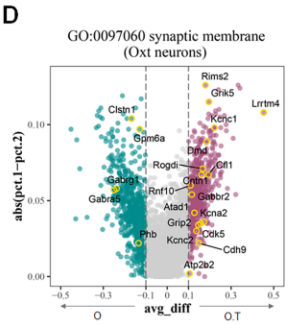

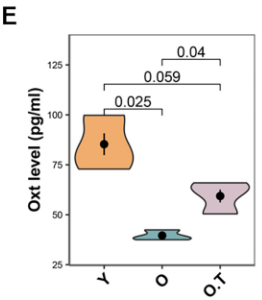

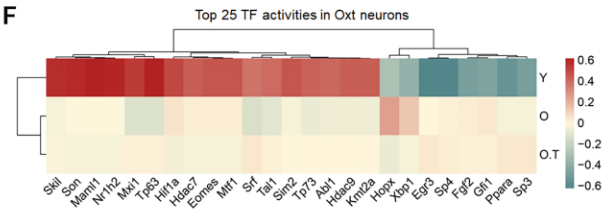

G

outcome	method	nsnp	OR(95%CI)	pval	Q_pval	pleiotropy.pval
Neurexophilin−1 || id:prot−a−2132	IVW	34	1.327 (1.223 to 1.439)	1e−11	0.12	0.05
Amyloid−like protein 2 || id:prot−a−123	IVW	34	1.264 (1.176 to 1.359)	2.4e−10	0.42	0.2
Pro−opiomelanocortin || id:prot−a−2327	IVW	68	1.147 (1.090 to 1.207)	1.6e−07	0.42	0.46
Agouti−signaling protein || id:prot−a−187	IVW	68	0.882 (0.837 to 0.930)	2.7e−06	0.32	0.11
Glucagon || id:prot−a−1181	IVW	34	1.124 (1.046 to 1.207)	0.0014	0.86	0.35
Insulin−like growth factor−binding protein 2 || id:prot−a−1448	IVW	34	1.124 (1.040 to 1.215)	0.0033	0.21	0.8
Cystatin C levels || id:ebi−a−GCST90025945	IVW	5	1.020 (1.006 to 1.035)	0.0045	0.54	0.88
Cystatin−F || id:prot−a−705	IVW	34	1.108 (1.031 to 1.190)	0.005	0.75	0.43
Cerebellin−1 || id:prot−a−371	IVW	34	0.899 (0.835 to 0.969)	0.0053	0.33	0.87
Neuropeptide W || id:prot−a−2082	IVW	68	0.932 (0.886 to 0.980)	0.006	0.98	0.31
Glial cell line−derived neurotrophic factor || id:prot−a−1198	IVW	34	1.105 (1.023 to 1.194)	0.011	0.24	0.57
Serpin A9 || id:prot−a−2694	IVW	34	1.113 (1.024 to 1.210)	0.012	0.078	0.4
Beta−endorphin || id:prot−a−2325	IVW	34	1.123 (1.025 to 1.229)	0.012	0.015	0.78
Total testosterone levels || id:ebi−a−GCST90012112	IVW	33	1.012 (1.002 to 1.021)	0.015	0.13	0.97
Thyroid Stimulating Hormone || id:prot−a−530	IVW	34	1.092 (1.016 to 1.172)	0.016	0.75	0.58
Progonadoliberin−1 || id:prot−a−1233	IVW	34	1.091 (1.016 to 1.172)	0.017	0.82	0.42
Insulin−like growth factor 1 levels || id:ebi−a−GCST90025989	IVW	5	0.984 (0.970 to 0.998)	0.025	0.71	0.29
Total Testosterone || id:ieu−b−4864	IVW	32	1.011 (1.001 to 1.020)	0.026	0.52	0.92
Thyroid hormone receptor alpha || id:prot−a−2974	IVW	34	1.085 (1.003 to 1.173)	0.041	0.2	0.56
Insulin−like growth factor−binding protein 1 levels || id:ebi−a−GCST90010221	IVW	30	1.148 (1.006 to 1.311)	0.041	0.29	0.92
Insulin−like 3 || id:prot−a−1560	IVW	34	1.106 (1.003 to 1.218)	0.043	0.0022	0.82
Growth hormone receptor || id:prot−a−1211	IVW	68	0.941 (0.887 to 0.999)	0.046	0.019	0.26

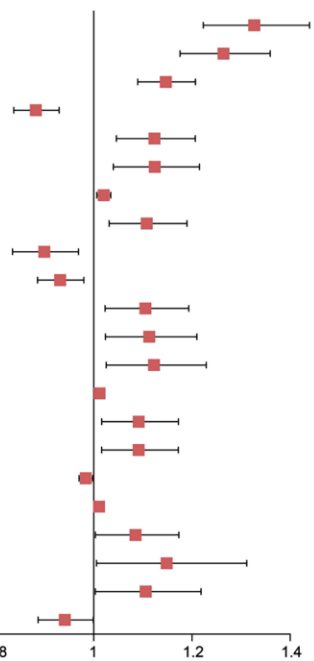

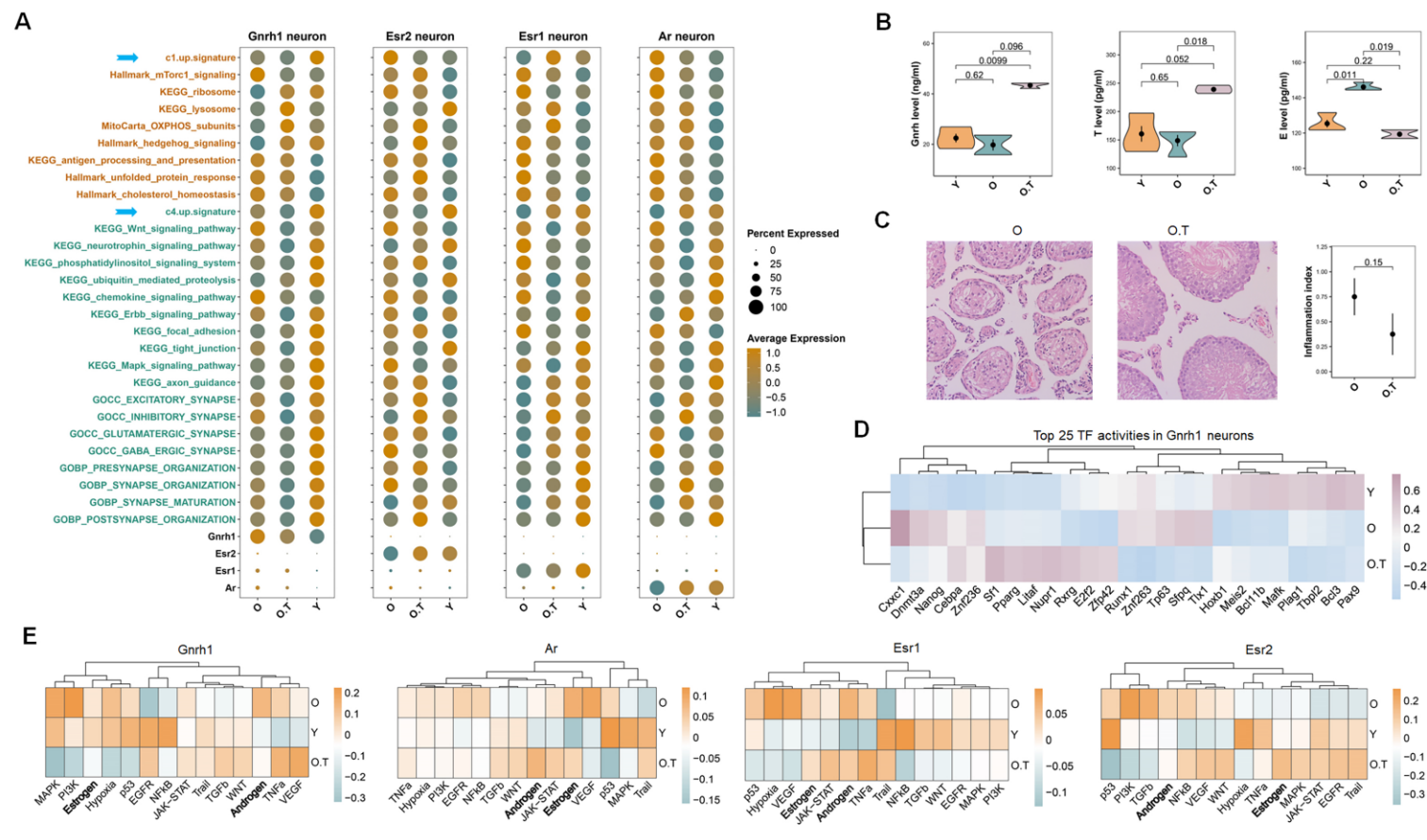

F

exposure	outcome	method	nsnp	OR(95%CI)	pval	Q_pval	pleiotropy.pval
GNRH1	Proenkephalin−A || id:prot−a−2247	IVW	48	1.336 (1.264 to 1.413)	1.9e−24	0.72	0.26
GNRH1	Proprotein convertase subtilisin/kexin type 7 || id:prot−a−2212	IVW	24	1.254 (1.159 to 1.357)	1.8e−08	0.51	0.95
GNRH1	Agouti−signaling protein || id:prot−a−187	IVW	48	1.218 (1.132 to 1.310)	1.3e−07	0.0015	0.31
GNRH1	Growth hormone receptor || id:prot−a−1211	IVW	48	0.863 (0.816 to 0.913)	2.3e−07	0.98	0.34
GNRH1	Galanin peptides || id:prot−a−1166	IVW	24	1.236 (1.133 to 1.349)	1.9e−06	0.2	0.93
GNRH1	Estrogen receptor || id:prot−a−991	IVW	24	1.222 (1.124 to 1.329)	2.8e−06	0.3	0.73
GNRH1	Pro−opiomelanocortin || id:prot−a−2327	IVW	48	1.139 (1.077 to 1.204)	4.8e−06	0.98	0.083
GNRH1	Insulin−like growth factor−binding protein 6 || id:prot−a−1450	IVW	24	1.232 (1.124 to 1.351)	8.7e−06	0.11	0.67
GNRH1	Beta−endorphin || id:prot−a−2325	IVW	24	1.184 (1.094 to 1.281)	0.000027	0.55	0.48
GNRH1	Brain−derived neurotrophic factor || id:prot−a−242	IVW	24	1.131 (1.045 to 1.223)	0.0022	0.63	0.91
GNRH1	Adrenomedullin || id:prot−a−48	IVW	24	1.271 (1.083 to 1.492)	0.0033	9.3e−11	0.72
GNRH1	Insulin−like growth factor−binding protein 1 levels || id:ebi−a−GCST90010221	IVW	22	0.820 (0.718 to 0.936)	0.0034	0.28	0.57
GNRH1	Prolactin receptor || id:prot−a−2377	IVW	24	1.124 (1.039 to 1.216)	0.0036	0.85	0.44
GNRH1	Insulin−like growth factor−binding protein 3 || id:prot−a−1449	IVW	24	0.883 (0.811 to 0.962)	0.0044	0.25	0.63
GNRH1	Early placenta insulin−like peptide || id:prot−a−1561	IVW	24	1.117 (1.032 to 1.208)	0.0059	0.58	0.58
GNRH1	Bradykinin, des−arg(9) || id:met−a−656	IVW	10	0.778 (0.641 to 0.943)	0.01	4.6e−31	0.071
GNRH1	Leptin receptor || id:prot−a−1724	IVW	24	1.097 (1.014 to 1.187)	0.021	0.98	0.42
GNRH1	Thyroid hormone receptor alpha || id:prot−a−2974	IVW	24	1.086 (1.004 to 1.176)	0.039	0.82	0.78

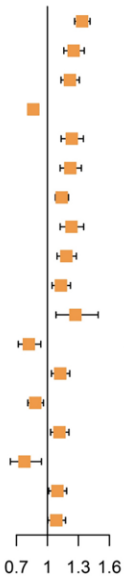

G
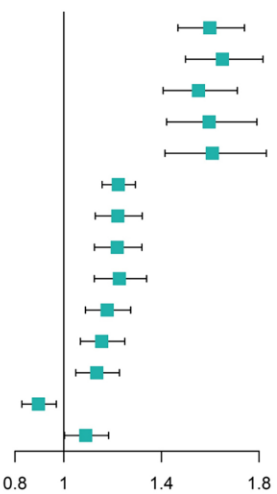
exposure	outcome	method	nsnp	OR(95%CI)	pval	Q_pval	pleiotropy.pval
GNRH1	Somatostatin−28 || id:prot−a−2846	IVW	24	1.598 (1.468 to 1.740)	4.1e−27	0.26	0.53
GNRH1	Chromogranin−A || id:prot−a−538	IVW	24	1.650 (1.499 to 1.816)	1.7e−24	0.06	0.5
GNRH1	Neuropeptide W || id:prot−a−2082	IVW	48	1.552 (1.407 to 1.711)	1.3e−18	4.8e−12	0.77
GNRH1	Protachykinin−1 || id:prot−a−2920	IVW	24	1.596 (1.421 to 1.791)	2.3e−15	0.001	0.89
GNRH1	Glucagon || id:prot−a−1181	IVW	24	1.609 (1.414 to 1.830)	4.5e−13	0.000021	0.98
GNRH1	Brain natriuretic peptide 32 || id:prot−a−2077	IVW	48	1.223 (1.157 to 1.294)	1.3e−12	0.9	0.026
GNRH1	Corticotropin || id:prot−a−2326	IVW	24	1.221 (1.129 to 1.322)	6.4e−07	0.79	0.73
GNRH1	Prolactin−releasing peptide || id:prot−a−2376	IVW	24	1.219 (1.126 to 1.320)	1.1e−06	0.43	0.089
GNRH1	Progonadoliberin−2 || id:prot−a−1234	IVW	24	1.228 (1.125 to 1.340)	4e−06	0.21	0.42
GNRH1	Secretogranin−1 || id:prot−a−539	IVW	24	1.178 (1.089 to 1.274)	0.000046	0.81	0.51
GNRH1	Atrial natriuretic factor || id:prot−a−2076	IVW	24	1.155 (1.068 to 1.250)	0.00032	0.57	0.56
GNRH1	Estradiol 17−beta−dehydrogenase 2 || id:prot−a−1383	IVW	24	1.135 (1.049 to 1.228)	0.0016	0.69	0.62
GNRH1	Insulin−like growth factor I || id:prot−a−1443	IVW	24	0.896 (0.828 to 0.970)	0.0063	0.95	0.48
GNRH1	Insulin−like growth factor 1 receptor || id:prot−a−1444	IVW	24	1.090 (1.003 to 1.184)	0.042	0.33	0.62